International journal of COMADEM
Vol 22 No 02 (April 2019) p.

COMADEM
International Journal of Condition Monitoring and Diagnostic Engineering Management

Effects of asymmetric flow within vaneless diffuser on the performance characteristics of the compressor stage of a turbocharger

Noukhez Ahmed [a]*, Taimoor Asim [b], Rakesh Mishra [c]

[a] *Faculty of Science and Engineering, University of Wolverhampton, Wulfruna Street, Wolverhampton, UK WV1 1LY*
[b] *School of Engineering, Robert Gordon University, Garthdee Road, Aberdeen, UK AB10 7GJ*
[c] *School of Computing and Engineering, University of Huddersfield, Queensgate, Huddersfield, UK HD1 3DH*

∗ *Corresponding author. Tel.: +44-190-232-2703*; *email*: *n.ahmed14@wlv.ac.uk*

ABSTRACT

Modern engines use turbocharger that provides the extra boost to the engines and hence helps in downsizing. Turbochargers comprise of the turbine stage, bearing housing and the compressor stage. Compressor Stage helps in providing compressed air to the engine resulting in possibility of increasing the fuel-to-air ratio, which may provide extra power to the engine. Diffuser is one of the major components within the compressor stage, which helps in increasing the pressure and hence the density of incoming air. The shape of the diffuser has a significant effect on the performance characteristics of the compressor stage. According to the studies found in the literatures, it has been found that the variations in velocity profiles within the diffusers have impact on total-to-total compressor stage performance. Therefore, it is essential to critically evaluate the effect of diffuser shape on the velocity profiles across the diffuser passage. Published literature is severely limited in establishing the effects of the velocity profile asymmetry across the diffuser on the performance characteristics of the compressor stage. Hence, the present study focuses on using a well-validated Computational Fluid Dynamics tool to numerically simulate the flow within the diffuser of various shapes quantified in form of an asymmetric effect on the performance of the compressor stage. Both straight wall diffuser and diverged wall straight diffuser have been investigated in the present study. A full factorial based DoE have been incorporated whereby two factors (L/L_{max} and b_2/b_1) have been selected respectively. Variations in flow related parameters within the diffuser have been discussed in detail for a wide range of geometrical parameters associated with the diffuser shape. It has been found in the analysis of this paper that flow across diffuser is highly asymmetric. Therefore, asymmetry of velocity profiles values has been used to predict the performance of the compressor stage as a function of radial and circumferential velocities across the diffuser. Furthermore, a novel semi-empirical prediction model has been developed to predict diffuser performance as a function of geometric and flow variables of the diffuser. The resulting diffuser map can be used for inverse design of diffuser for compressor stage as well.

Keywords: *Computational Fluid Dynamics (CFD); Turbomachinery; Compressor stage; Vaneless diffuser; Asymmetric ratio.*

1. Introduction

International legislation requires sustained lowering of the emissions and the fuel consumption in internal combustion engines. Reducing the fuel consumption without sacrificing the level of performance delivered by the current vehicles has become a challenge for automotive industries. Turbocharging is one of the solutions to reduce emission levels by utilising the exhaust gas energy. The turbocharger's performance is explicitly dependent upon the compressor stage efficiency. The compressor stage efficiency is further dependent upon the flow characteristics within the different components of the compressor, especially the diffuser passage. Diffuser plays a significant role in increasing the stage efficiency. However, the flow variations within the diffuser are dependent upon the incoming flow from the impeller. Estimation of local flow variations across the diffuser is very difficult as these depend on the shape and number of blades used in the impeller. Currently the performance characteristics of compressor stage are defined by the total-to-total stage isentropic efficiency as per equation (1). It has been found in literature that the compressor stage components in general and diffuser in particular have impact on the total-to-total stage performance.

$$\eta_t = \frac{T_{o,in} \times \left[PR_C^{\frac{\gamma-1}{\gamma}} - 1 \right]}{T_{o,out} - T_{o,in}} \quad (1)$$

Japikse and Goebel [1] have carried out experimental studies to develop techniques in order to estimate the flow behaviour within the compressor stage, focusing on the diffuser passage. It has been found that when the flow enters a straight diffuser, it follows the hub wall of the passage at the impeller discharge due to the impeller passage direction. Backflow appears near the shroud wall of the diffuser passage. This flow behaviour reverses midway to the diffuser passage, whereby the flow attaches the shroud surface after the midway and backflow is obtained near the hub wall. Adachi et al. [2] have carried out experiments to improve the performance of the vaneless diffuser passage of a compressor stage. This study focused on the optimisation methods for annular vaneless diffusers for improving the overall compressor stage performance. The aim of this investigation was to improve both the surge margin and isentropic efficiency at

high flow rates. The results show that reducing the diffuser outlet width (by tapering the passage) increases the surge margin. However, if the outlet section of the diffuser passage becomes too small, the mass flow rate increases, which reduces the static pressure and leads to decrease in the isentropic efficiency.

Lee and Bein [3] invented a new diffuser geometry to improve the performance of the compressor stage. The shroud wall of the diffuser passage is made to converge and diverge in contouring format. This design has been estimated by reducing recirculation obtained across the diffuser passage. Minimum recirculation causes higher static pressure recovery has led to best diffuser model. This approach increases the stage isentropic efficiency by 3%. Turunen-Saaresti et al. [4] conducted experimental and numerical investigations on the vaneless diffuser of a centrifugal compressor, consisting of an unshrouded impeller and volute. Eight different configurations of diffusers, with various pinch heights and their respective locations, have been numerically investigated and validated with the experimental data. Compressor stage performance has been analysed, for each diffuser configuration, for the overall efficiency, circumferential static and total pressure and span wise total pressure distribution (before and after the diffuser). The numerical models have shown pressure ratio results, which are in good agreement with the experimental data, however, it over-predicts the isentropic efficiency. Both experimental and numerical results show that the pinched diffuser increases the compressor efficiency because of reduced temperature variations. Furthermore, the pinch on the shroud wall depicts higher efficiency as compared to the pinch on the hub wall because increased critical flow angle at the diffuser inlet. Pinching both the walls together ensures optimal compressor and diffuser performance.

Jaatinen et al. [5] studied the effect of the diffuser width variations on the performance of the compressor and the diffuser. The performance of the compressor, in terms of efficiency and total-to-total pressure ratio, has been calculated for six different diffuser configurations, having varying widths. For the first three configurations, the width was reduced from the shroud wall, while for the other three configurations; the width was reduced from both hub and the shroud walls. It has been found that pinching the shroud wall yields higher efficiency, by reducing the tip clearance flow losses. It is further concluded from this investigation that the shroud pinch should be greater than the tip clearance for narrow diffusers.

Mohtar et al. [6] conducted a series of experimental investigations aiming to study the effect of the Map Width Enhancement MWE design on the compressor performance and surge extension. Compressor cover with the slotted groves is referred as MWE, which helps to improve the surge margin by recirculating the reverse flow to the impeller inlet when surging initiates. Different configurations of the turbocharger compressor stage have been considered in these investigations. One of the approaches used in this study is pinching the shroud wall of the diffuser, while the other approach increases the diffuser area. The total-to-total compressor stage efficiency, and surge margin, has been investigated in both the cases. Results show that at low rotational speeds, the pinch on the shroud wall increases the surge margin, but at high rotational speeds, the pinch has less effect on the surge margin. The stage efficiency has been found to decrease as the mass flow rate increases.

Robinson et al. [7] conducted numerical investigations on a single stage centrifugal compressor having a vaned diffuser. In this investigation, the impeller-diffuser spacing was reduced from 15% to 7% of the impeller tip radius. The overall efficiency, pressure fluctuation in the impeller, blade surface pressure at the impeller exit, and the pressure recovery (C_p) has been quantified using the transient approach. The results of the reduced diffuser area model have been compared against the baseline model. According to the findings, the compressor with reduced diffuser width improves the stage efficiency by 1%.

Jaatinen et al. [8] conducted experimental investigations on three vaneless diffusers with different width, along with four different tip clearances. The overall stage performance and the flow field within the diffuser have been investigated by analysing the radial velocity and flow angle for each case. The results show that a moderate pinch enhances the compressor overall efficiency, reducing the losses in the diffuser. However, excessive pinch has negative effects on the efficiency due to the flow separation. Moreover, reducing the flow area across diffuser increases the flow acceleration, which reduces the boundary layers, resulting in lower boundary layer losses. A 2% increase in the efficiency has been recorded at the design point, and approximately 3% efficiency increase is recorded at higher mass flow rates. Almost at the same time, Sheng et al. [9] studied the effects of unparalleled diffuser walls on the generation of rotating wave in a centrifugal compressor. Five diffuser configurations (convergent, convergent and divergent, and tapered shroud wall) have been investigated and compared against a parallel wall diffuser (i.e. baseline model). The critical inlet flow angle and the rotating wave speed have been analysed at various diffuser inlet Mach numbers and diffuser outlet-to-inlet radius ratios. The tapered shroud wall contraction increases the suppression effect on the rotating stall in the diffuser. The suppression effect has been found to be dependent on various parameters, such as diffuser inlet Mach number, diffuser width-to-inlet ratio, diffuser inlet-to-outlet ratio and contraction shape. It has been noticed that the unparalleled wall diffuser maintains the flow stability at high Mach numbers. Moreover, while the convergent and divergent wall diffusers provide higher stability at low inlet Mach numbers, the convergent wall configuration seems to provide stability at higher Mach numbers. The Bezier curved shroud wall improves the diffuser stability, and its effects depend on the inlet Mach number.

Schiff [10] developed a computer program to design a radial compressor and analyse the flow field within the impeller and the diffuser. The author has considered one impeller configuration, three vaneless diffuser configurations, and a vaned diffuser configuration to analyse the performance of the compressor stage. The velocity profile has been analysed along the diffuser. It has been noticed that the converging diffuser model yields improved diffuser stability and higher efficiency.

Jaatinen et al. [11] carried out numerical investigations on a centrifugal compressor with vaneless diffuser to investigate the effect of variation of diffuser width on the compressor performance. Seven vaneless diffusers have been investigated, with diffuser width ratio of 0.5 to 1. Entropy change in the impeller, and the velocity profile, have been analysed to predict the compressor stage performance. The results show that for the given compressor stage, a moderate pinch on the shroud wall (ranging b/b_2= 0.85–0.91) is beneficial. The pinch reduces the tip clearance flow losses, making the flow uniform, and hence reducing the entropy and enhancing the performance. However, excessive pinching increases the velocity, making the flow field unstable. This causes flow separation near the shroud wall, which increase the entropy. The amount of flow separation depends on the shape of the pinch and the way it is implemented.

Achilleos [12] performed numerical investigations on a centrifugal compressor to optimise the diffuser geometry for optimal compressor stage performance. The shroud of the diffuser wall has been diverged at the diffuser outlet. Various configurations have been analysed by changing the divergence angle and its location. The results show that a diverged shroud wall causes an increase in the diffuser outlet width, which improves the stage efficiency, and total-to-total pressure ratio, at low mass flow rates. However, at higher mass flow rates, both efficiency and pressure ratio decreases.

Shaaban [13] conducted numerical investigations aiming to improve the performance of a radial compressor by reducing the diffuser loss coefficient and increasing the pressure coefficient. The author has proposed two diffuser models with convergent and divergent shroud walls. The 3D numerical simulations show that the optimised model enhances the compressor performance by reducing the loss coefficient (by 4.7%). This increases the pressure coefficient by 6.6% under wake and swirl flow conditions.

Critical analyses of the published literature regarding the flow behaviour within the valueless diffuser and its performance characteristics reveal that these analyses are carried out mostly on the global performance parameters of the compressor stage or local diffuser shape modifications and its effect onto the total-to-total efficiency of the compressor. However, a better understanding of the local flow phenomena and its profile characteristics on the local performance parameters is extremely important in order to ensure better performance characteristics at design and off-design conditions. In the present study, local flow field analyses within the diffuser has been carried out at various design points, in order to estimate the contribution of various geometrical features of the diffuser and its local performance. Furthermore, the contributions of other compressor components, such as inlet with Map Width Enhancement (MWE) duct, impeller and volute, have also been enumerated. CFD based analysis have been carried out in the present study to analyse the flow distribution within the different sections of the diffuser, which affects the local flow profile across the diffuser. Moreover, the effect of local flow profile on the local diffuser performance has also been analysed in detail.

2. Numerical Modelling of Compressor Stage

A compressor stage available with the corresponding author, which is used in turbocharger has been has been numerically modelled, as shown in figure 1. The turbocharger compressor stage comprises of an inlet duct, MWE, impeller, vaneless diffuser, an overhung volute and a discharge duct. The impeller of the turbocharger compressor stage consists of seven full and seven splitters backward swept blades. In order to maintain fully developed flow conditions, a pipe section has been attached to the inlet duct. The entrance length is much shorter in turbulent flows and its dependence on the Reynolds number is weak. In many practical engineering applications, the inlet flow gets developed within the pipe length of 10D, where D represents diameter. The same has been considered in the present study as well [14].

Selection of mesh schemes affects the accuracy of prediction using numerical schemes. Cox [15], Cox et al. [16] and Sbardella et al. [17] have used different types of mesh schemes; structured mesh and unstructured mesh and a combination of structured and unstructured mesh called hybrid mesh on the turbomachines to investigate the feasibility and accuracy of the results. The results show that unstructured mesh in the axial and tangential directions offers more flexibility than standard structured meshes, both in terms of skewness and smoothness. The solution obtained using semi-unstructured mesh (hybrid mesh) seems to be superior to the structured mesh in terms of convergence rate.

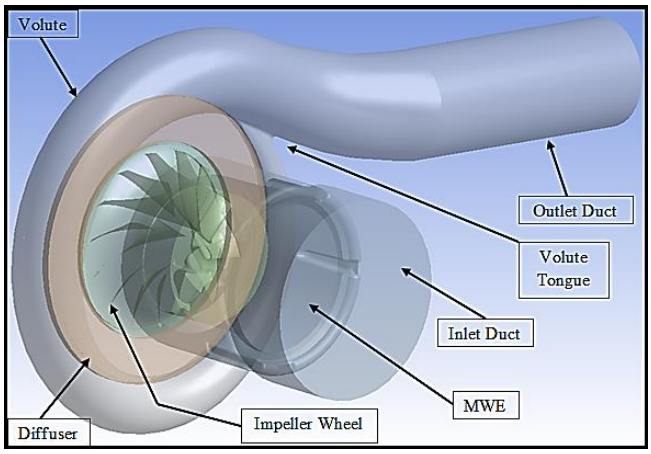

Figure 1. Geometry of the turbocharger compressor stage

Based on the literature, hybrid mesh has been employed within the compressor stage, in the present study. The structured mesh has been specified in the near-wall region and around the impeller blades. An unstructured mesh has been generated in the remaining flow domain. ICEM software has been used to generate the hybrid mesh within the compressor stage components for flow discretization. A mesh smoothing procedure has been used for each of the mapped radial layers, to minimize grid skewness. The smoothing procedure includes the movement of the points around the leading and the trailing edges to preserve high resolution mesh on the blade curvatures [18]. The volume mesh within the flow domain has been created, followed by the hexahedral mesh near the walls. The mesh quality has been checked after the generation of the mesh.

Grid sensitivity study has been carried out to ascertain that the numerical predictions are independent of mesh size used. This has been carried out by systematically increasing the number of elements used within the compressor stage, and monitoring the stage efficiency, as reported in a number of studies [19-26]. A list of cases used to investigate the mesh independency effects are presented in table 1.

Table 1. Grid sensitivity testing for the turbocharger compressor stage

Number of Cells Millions	Efficiency (T-T) (%)	Ratio of Efficiency (T-T) to Design Efficiency (-)
4.6	63.9	0.89
5.6	69.7	0.97
6.6	70.4	0.98
8.6	66.0	0.92
10.6	70.9	1.00
12.6	70.8	1.00

These results show that the flow parameters are independent of mesh density after 10.6 million elements, and hence, 10.6 million mesh elements are used to carry out further analysis in the present study.

3. Theoretical Background

This section describes the application of boundary condition required to simulate the centrifugal compressor. Similar, turbulence model and software package required to simulate has been detailed in this section of the paper.

3.1. Solver Execution

Specification of appropriate boundary conditions is critical to the accuracy of numerical analysis. Ansys CFX has been used to simulate the flow of air within the compressor stage. Ideal gas equation for the flow of air within the compressor stage has been used to analyse the compressibility effects. A steady state solver has been employed, along with the appropriate boundary conditions and the interface models.

Table 2. Boundary conditions applied to the turbocharger compressor stage

Boundary Name	Domain / Boundary Type	Boundary Condition
Inlet	Pressure Inlet	1 atm
	Temperature Inlet	288 K
	Operating (Reference) Pressure	0 atm
Outlet	Pressure Outlet	Variable
Impeller	Rotating	No-Slip
MWE	Stationary	No-Slip
Diffuser	Stationary	No-Slip
Volute	Stationary	No-Slip

In the present study, the fluid medium within the centrifugal compressor stage is compressible. The boundary types, and their corresponding values, have been summarised in table 2. The inlet pressure remains constant at 1atm throughout this study, mimicking the normal atmospheric pressure. A total temperature of 288K is specified at the inlet. Furthermore, the walls of the flow domain have been modelled as no-slip boundaries (as observed in real world conditions). The compressor stage has been numerically simulated at two operational speeds with four design points of the compressor map each as presented in table 3.

Table 3. Outlet boundary conditions

Rotating Speed $rpsK^{-1/2}$	Pressure Ratio (T-T) -
58.9	1.31
58.9	1.51
58.9	1.55
58.9	1.60
78.6	1.57
78.6	2.00
78.6	2.10
78.6	2.16

The flow within the compressor stage is highly turbulent. Jaatinen [27] has carried out research on the performance improvement of the centrifugal stage with pinched geometry vaned diffuser. Two different turbulence models i.e. Chien's k-ε and k-ω SST models, have been used to investigate the flow characteristics locally within the diffuser passage of the compressor stage. It has been observed that the k-ω SST turbulence model predicts the performance and the flow field across the impeller and diffuser passages with higher accuracy as compared to the standard k-ε model. Hence, k-ω SST turbulence model has been used in the study for the flow field analysis within the centrifugal compressor stage.

Getting to a converged solution is necessary in numerical simulations. A converged solution indicates that the solution has reached a stable state and the variations in the flow parameters, w.r.t. the iterative process of the solver, have died out. The default convergence criterion for the continuity equation, velocities in three dimensions and the turbulence parameters is 10^{-6}. In the present study, the total-to-total pressure ratio (outlet-to-inlet) and the mass flow rate (at both the outlet and the inlet) have been monitored during the iterative process. The solution has been considered converged once the total-to-total pressure ratio and the mass flow rate have become stable/constant.

4. Analysis

Numerical simulations have been carried out to analyse the flow behaviour across the diffuser of the centrifugal compressor stage. However, to justify the quality of simulations, the results have been verified with experimental data. These analyses have been detailed in this section of the paper.

4.1. Verification of Numerical Results

In order to ascertain the accuracy of the numerical modelling and the solver settings used in the present study, numerical predicted results need to be verified against the experimental findings. In the present study, this has been carried out on total-to-total stage pressure ratio and total-to-total stage isentropic compression efficiency as depicted in figure 2 and figure 3. It can be seen that numerical predicted results match closely at design conditions and off-design conditions at both operational speeds. The results are obtained at lower operational speeds for the compressor stage because high efficiencies are obtained at these conditions. It can be seen that at the speed of $58.9rpsK^{-1/2}$, the differences in the mass flow rate and the pressure ratio are 0.0% and 0.74%, this condition being near surge condition. Similarly, the differences in the mass flow rate and pressure ratio are less than 3.85% and 2.30% at Best Efficiency Point (BEP). Moreover, the differences in the mass flow rate and pressure ratio are 8.8% and 4.32% at the near choke condition. Furthermore, it can also be seen that at the speed of $78.6rpsK^{-1/2}$, the differences in the mass flow rate and pressure ratio are 0.0% and 0.11% at near surge condition. Similarly, differences in the mass flow rate and pressure ratio are less than 5.46% and 7.55% at BEP. Moreover, the differences in the mass flow rate and pressure ratio are 10.35% and 6.46% at near choke condition.

Figure 3 depicts the comparison of numerically simulated results and the experimental data, using plot of variation of efficiency - efficiency against mass flow rate variations (from choke line to surge line) at operational speeds of $58.9rpsK^{-1/2}$ and $78.6rpsK^{-1/2}$. It can be seen that at operational speed of $58.9rpsK^{-1/2}$, the differences in the mass flow rate and efficiency are 0.0% and 0.82% at near surge condition. Similarly, differences in the mass flow rate and efficiency are less than 3.85% and 6.30% at BEP. Moreover, the differences in the mass flow rate and efficiency are 8.8% and 8.19% at near choke condition. Furthermore, it can also be seen that at operational speeds of $78.6rpsK^{-1/2}$, the differences in the mass flow rate and efficiency are 0.0% and 1.57% at near surge condition. Similarly, the differences in the mass flow rate and efficiency are less than 5.46% and 7.42% at BEP. Moreover, the differences in the mass flow rate and efficiency are 10.35% and 4.97% at near choke condition. It can be seen that the numerical results match reasonably well with the experimental data. The mass flow rate is verified with the results under 4% in design conditions and under 11% in off-design conditions. Furthermore, the total pressure ratio is verified with the results under 8% in design conditions and under 7% in off-design conditions. Moreover, efficiency is verified with the results under 9% in design conditions and under 8% in off-design conditions. The variations in mass-flow rate and static pressure in design conditions are in good agreement with experimental results. However, the variations in mass-flow rate and static pressure in off-design conditions are a bit higher

because the numerical data has been obtained using steady state analysis, which overshoots the results in off-design conditions.

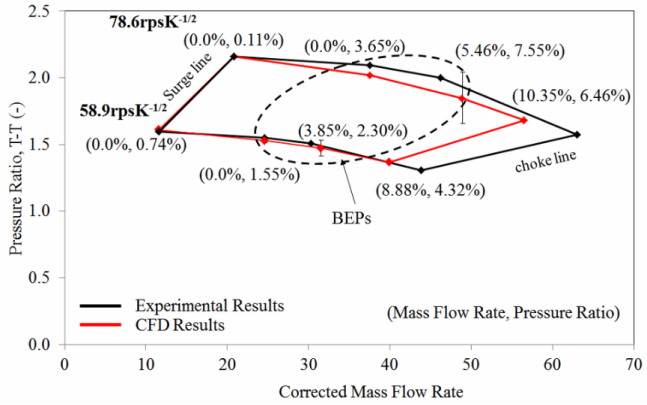

Figure 2. Verification of the numerical results with experimental data using pressure ratio and mass flow rate at operational speeds of 58.9rpsK$^{-1/2}$ and 78.6rpsK$^{-1/2}$

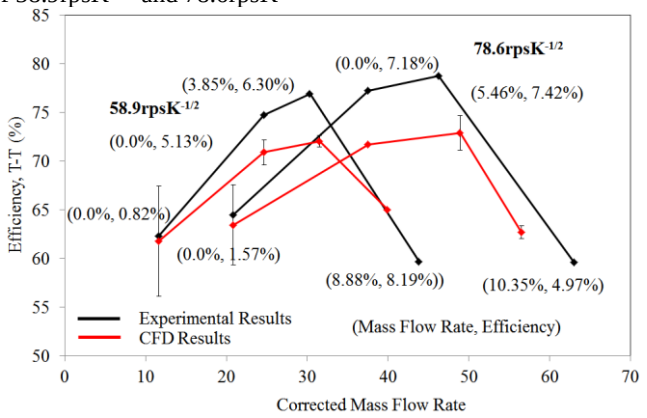

Figure 3. Verification of the numerical results with the experimental data using plot of variation of efficiency (T-T) mass flow rate at operational speeds of 58.9rpsK$^{-1/2}$ and 78.6rpsK$^{-1/2}$

4.2. Performance Characteristics of Straight Wall Diffuser

In the present study, the analysis of the diffuser is presented systematically in various sections. Firstly, the profiles of velocity vectors will be presented. Thereafter, statistical calculations have been carried out which define the velocity profiles across the diffuser. Furthermore, a novel parameter (an asymmetric ratio) has been used to describe the flow field within the diffuser. This procedure has been carried out at the two operational speeds; 58.9rpsK$^{-1/2}$ and 78.6 rpsK$^{-1/2}$ in order to find out the effect of asymmetry on the local performance and how asymmetry changes at design and near off-design conditions. This analysis explains the significance of velocity vectors on the performance and then semi-empirical equations have been created, which are dependent upon the velocity vector.

The velocity profiles have been created and presented at different sections of the diffuser. Figure 4 depicts five locations across the vaneless diffuser, ranging from L_1 to L_5, where L_1 represents 0% (diffuser inlet), L_2 represents 25%, L_3 represents 50%, L_4 represents 75% and L_5 represents 100% (diffuser outlet). 100 points are created from the hub wall to the shroud wall at each aforementioned location, to capture the flow velocity profiles across the diffuser. This helps in explaining the effect of asymmetric ratio on the performance of the diffuser at design and near off-design conditions and quantify non-uniformity in the flow field across the diffuser.

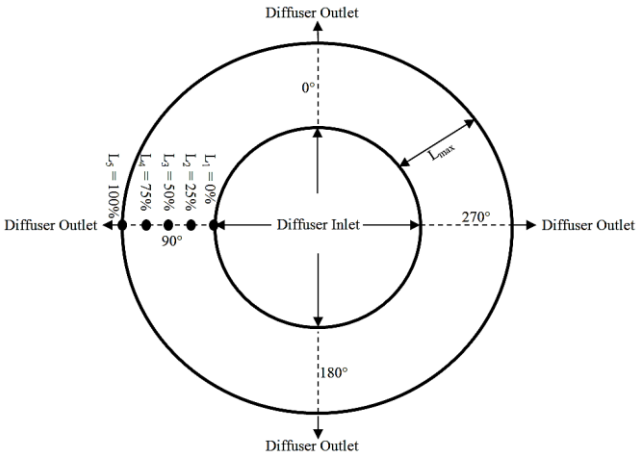

Figure 4. Points locations across the vaneless diffuser

Figure 5 depicts the velocity magnitude distribution across the diffuser from the hub wall to the shroud wall at BEP having an operational speed of 58.9rpsK$^{-1/2}$. In the figure, b_2/b_1 = 0 represents the hub wall of the diffuser and b_2/b_1 = 1 represents the shroud wall of the diffuser. It can be seen that the velocity magnitude is reduced radially across the diffuser having a maximum velocity of 206m/s at the diffuser inlet and 149m/s at the diffuser outlet. The velocity at the hub and the shroud walls is 0m/s because of no-slip wall boundary condition. Furthermore, it can also be seen that the local velocity magnitude is higher near the shroud wall and lower near the hub wall. Moreover, it can also be seen that as the flow moves across the diffuser, the velocity magnitude near the shroud wall reduces as well. However, the detailed analysis has been carried out by quantifying the asymmetric ratio for the velocity magnitude profile across the diffuser and has been presented in the upcoming sections.

A set of data has been obtained from the velocity profiles at 10%, 20%, 30% and 40% distance from the centreline towards the hub and the shroud walls (shown in figure 6). These values aid to obtain the local asymmetric ratio, α from the centreline towards the walls and from the diffuser inlet to the diffuser outlet, which is explained as follows:

$$\alpha = \frac{\text{Velocity at the top}}{\text{Velocity at the bottom}} \qquad (2)$$

The velocity magnitude across the diffuser is explained using asymmetric behaviour of the velocity profiles. A ratio of the velocity magnitude values is obtained at 10%, 20%, 30% and 40% distance from the centreline of the diffuser to the walls and 0% (diffuser inlet), 25%, 50%, 75% and 100% (diffuser outlet) distance from the diffuser inlet to the diffuser outlet. Figure 7 depicts the local asymmetric ratio for the velocity magnitudes, α_{vm} across the diffuser at BEP at an operational speed of 58.9rpsK$^{-1/2}$. α_{vm} values of 1.0 show that the flow is symmetric, α_{vm} values below 1.0 shows asymmetric flow towards the hub wall and α_{vm} values above 1.0 shows asymmetric flow towards the shroud wall. It can be seen that the flow is asymmetric towards the shroud wall across the straight diffuser. The asymmetric ratio for the velocity magnitude increases from the centreline of the straight diffuser towards the wall and from the diffuser inlet to the diffuser outlet.

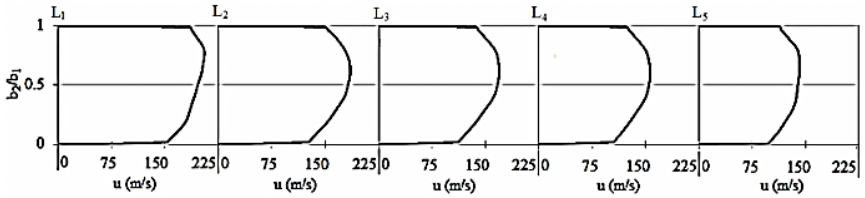

Figure 5. Velocity magnitude (m/s) distribution across the diffuser from the hub wall to the shroud wall at BEP at an operational speed of 58.9rpsK$^{-1/2}$

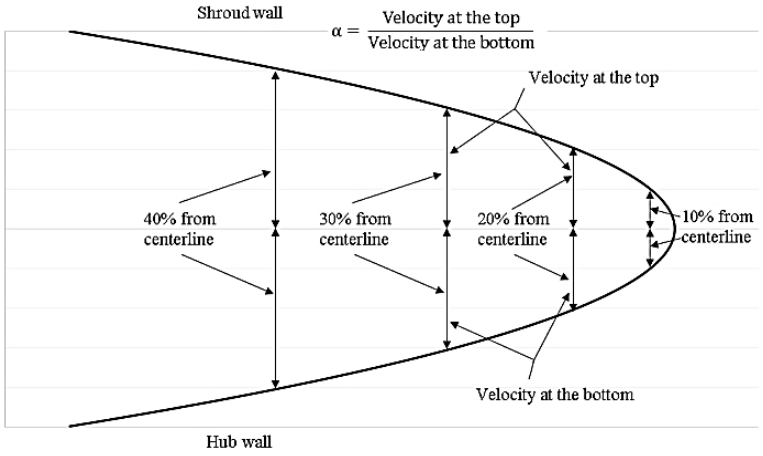

Figure 6. Velocity profile

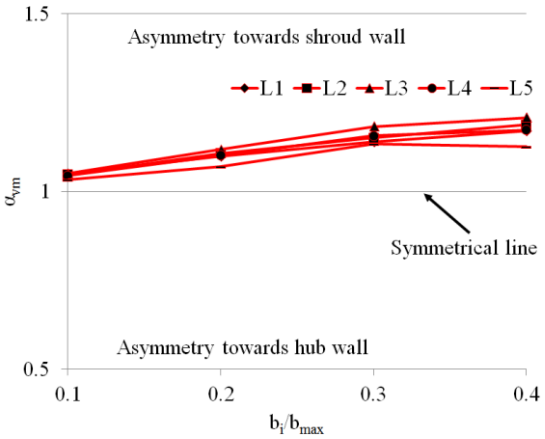

Figure 7. Verification of the numerical results with the experimental data using plot of variation of efficiency (T-T) mass flow rate at operational speeds of 58.9rpsK$^{-1/2}$ and 78.6rpsK$^{-1/2}$

Figure 8 depicts the comparison of velocity magnitude distribution across the centreline of the diffuser at the design condition and near off-design conditions at an operational speed of 58.9rpsK$^{-1/2}$. It can be seen that the velocity magnitude at the diffuser inlet is similar at near choke condition in comparison to that at BEP, whereas the velocity magnitude is higher at near surge condition in comparison to that at BEP. Furthermore, the velocity magnitude is almost similar at L_2 at both near choke condition and surge condition in comparison to that at BEP. Thereafter, the velocity magnitude is decreased at L_4 and L_5 (diffuser outlet) at near choke condition in comparison to that at BEP. However, the velocity magnitude is increased at L_4 and L_5 (diffuser outlet) at near surge condition in comparison to that at BEP. The detailed analysis has been carried out by quantifying the asymmetric ratio for the velocity magnitude profile across the diffuser at design and near off-design conditions.

Figure 9 depicts the local asymmetric ratio for the velocity magnitudes, α_{vm} across the diffuser at near off-design conditions at an operational speed of 58.9rpsK$^{-1/2}$. It can be seen that the flow is near symmetrical line (centreline across diffuser), showing less asymmetric ratio for the velocity magnitude at near choke condition in comparison to that BEP because of high mas flow rate. Furthermore, it can be seen in figure 9(b) that the flow is asymmetric at near surge condition across the diffuser. However, the asymmetric ratio is higher than 1.0 at L_1 (diffuser inlet) and L_2, showing asymmetry towards the shroud wall and the asymmetric ratio is lower than 1.0 at L_3, L_4 and L_5 (diffuser outlet), showing asymmetry towards the hub wall. Moreover, it can be seen that at L_5 (diffuser outlet) and 40% away from the centreline of the diffuser, the asymmetric ratio is nearly 0.5 at near choke condition and at near surge condition. This is because the diffuser wall is diverged near the diffuser outlet, which causes increase in the area ratio and hence has a significant effect on the asymmetric ratio.

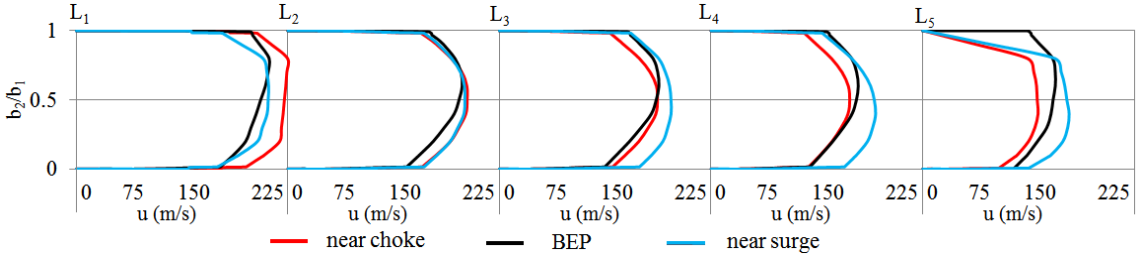

Figure 8. Comparison of velocity magnitude (m/s) distribution across the centreline of the diffuser at an operational speed of 58.9rpsK$^{-1/2}$ between design condition (BEP) and off-design conditions (at near choke and at near surge conditions)

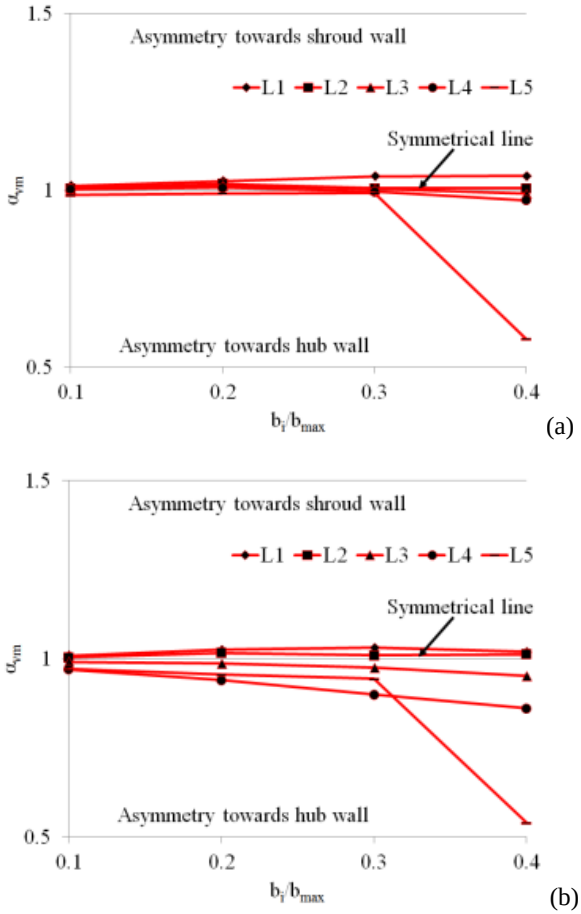

Figure 9. Local asymmetric ratio for the velocity magnitude, α_{vm} across the diffuser at design condition and at near off-design conditions at an operational speed of 58.9rpsK$^{-1/2}$

Figure 10 depicts the velocity magnitude distribution across the diffuser from the hub wall to the shroud wall at BEP at an operational speed of 78.6rpsK$^{-1/2}$. It can be seen that the velocity magnitude is reduced radially across the diffuser having a maximum velocity of 264m/s at the diffuser inlet and 195m/s at the diffuser outlet. The velocity at the hub and the shroud walls is 0m/s because of no-slip wall boundary condition. Furthermore, it can be seen that the velocity magnitude is higher near the shroud wall and lower near the hub wall. Moreover, it can also be seen that the flow across the diffuser asymmetric. However, the detailed analysis has been carried out by quantifying the asymmetric ratio for the velocity magnitude profile across the diffuser.

The behaviour of velocity magnitude across the diffuser is explained using symmetric and asymmetric behaviour of the velocity field profiles. Figure 11 depicts the local asymmetric ratio for the velocity magnitudes, α_{vm} across the diffuser at BEP at the operational speeds of 58.9rpsK$^{-1/2}$ and 78.6rpsK$^{-1/2}$. It can be seen that the flow is asymmetric towards the shroud wall across the straight diffuser. The asymmetric ratio is increasing from the centreline to the wall at BEP at an operational speed of 78.6rpsK$^{-1/2}$ similar to that at an operational speed of 58.9rpsK$^{-1/2}$. Same trend is found across the straight diffuser from diffuser inlet to diffuser outlet at an operational speed of 78.6rpsK$^{-1/2}$ in comparison to that at an operational speed of 58.9rpsK$^{-1/2}$.

Figure 12 depicts the comparison of velocity magnitude distribution across the centreline of the diffuser at the design condition and off-design conditions at an operational speed of 78.6rpsK$^{-1/2}$. It can be seen that the velocity magnitude at the diffuser inlet is higher at near off-design conditions in comparison to that at BEP. Furthermore, the velocity magnitude is almost similar at L_2 at both near choke condition and surge condition in comparison to that at BEP. Thereafter, the velocity magnitude is decreased at L_4 and L_5 (diffuser outlet) at near choke condition in comparison to that at BEP. However, the velocity magnitude is increased at L_4 and L_5 (diffuser outlet) at near surge condition in comparison to that at BEP. The detailed analysis has been carried out by quantifying the asymmetric ratio for the velocity magnitude profile across the diffuser at design and near off-design conditions. This will help to obtain the effect of asymmetric ratio for the velocity magnitude on the design and off-design conditions.

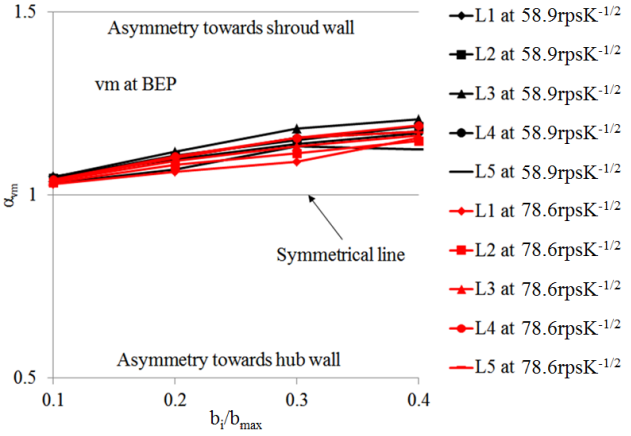

Figure 11. Local asymmetric ratio for the velocity magnitude, α_{vm} across the diffuser at BEP at the operational speeds of 58.9rpsK$^{-1/2}$ and 78.6rpsK$^{-1/2}$

Figure 13 depicts the comparison of local asymmetric ratio for the velocity magnitudes, α_{vm} across the diffuser at off-design conditions between the operational speeds of 58.9rpsK$^{-1/2}$ and 78.6rpsK$^{-1/2}$. It can be seen that the flow is highly asymmetric having asymmetric ratio less than 1.0 at near choke condition as depicted in figure 13(a). The flow is asymmetric towards the hub wall and it is increasing across the diffuser from L_1 (diffuser inlet) to L_5 (diffuser outlet). This is because the flow angle at the diffuser inlet does not align with the centreline is increased towards shroud wall.

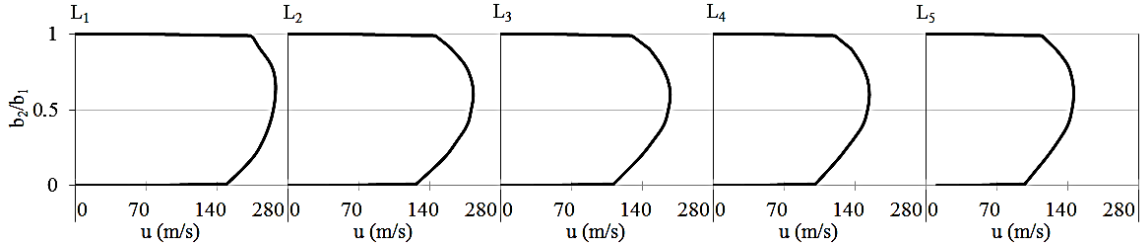

Figure 10. Velocity magnitude (m/s) distribution across the diffuser from the hub wall to the shroud wall at BEP at an operational speed of 78.6rpsK$^{-1/2}$

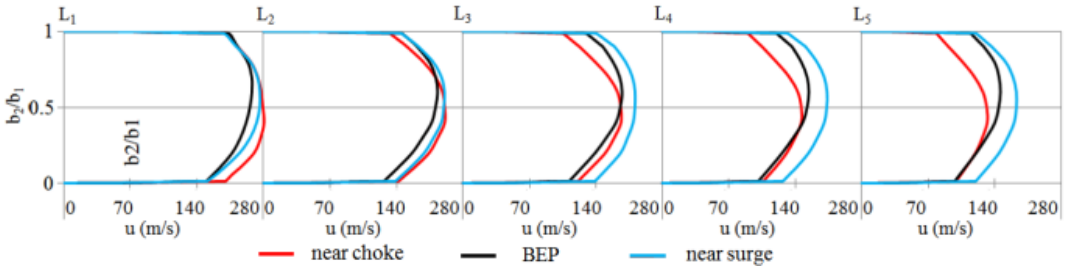

Figure 12. Comparison of velocity magnitude (m/s) distribution across the centreline of the diffuser at an operational speed of 78.6rpsK$^{-1/2}$ between design condition (BEP) and off-design conditions (at near choke and at near surge conditions)

Furthermore, it can be seen in figure 13(b) that the flow is asymmetric at near surge condition across the diffuser. However, the asymmetric ratio is higher than 1.0 across the width of the diffuser, which shows asymmetry towards the shroud wall. However, the asymmetric ratio is decreasing from L_1 (diffuser inlet) to L_5 (diffuser outlet) in comparison to that at an operational speed of 58.9rpsK$^{-1/2}$. Therefore, it can be concluded that the geometrical features of a flow path significantly influence the flow behaviour across the diffuser.

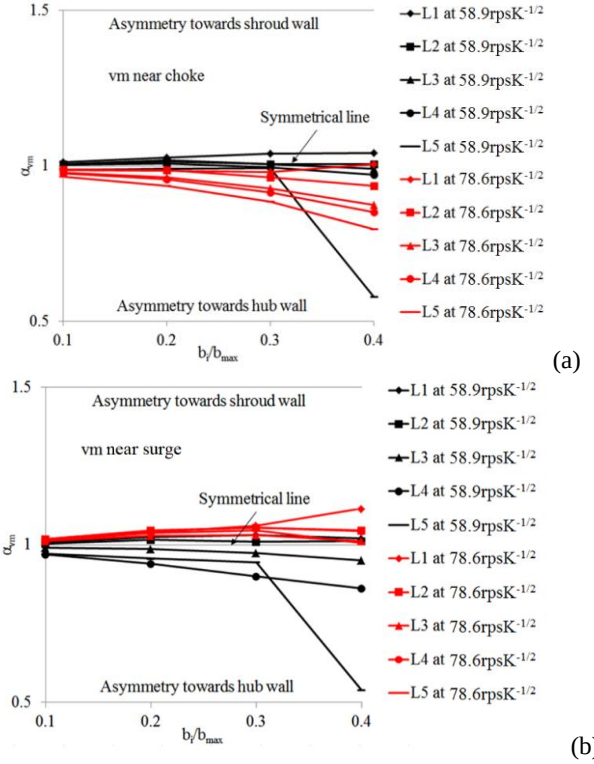

Figure 13. Local asymmetric ratio for the velocity magnitude, α_{vm} across the diffuser at design condition and at near off-design conditions at the operational speeds of (a) 58.9rpsK$^{-1/2}$ and (b) 78.6rpsK$^{-1/2}$

4.3. Performance Characteristics of Diverged Wall Diffuser

Many researchers have carried out various investigations to improve the compressor stage performance either by pinching, converging or diverging the diffuser walls as described in previous sections. Similar approach is used in this section as well to identify the effects of the wall divergence on the performance of the compressor stage. Furthermore, in this study the effect of wall divergence on the local flow variations are also investigated. Parametric investigations have been carried out to analyse the flow field characteristics within the diverged wall vaneless diffuser. To carry out the parametric investigations a Full Factorial based Design of Experiments (DoE) technique has been employed in the present study to determine the possible practical combinations of the geometrical parameters. Minitab 17 Statistical Software has been used in the present study to carry out Full Factorial based DoE studies, where a practical range of different parameters has been specified. The factors/parameters considered for the diffuser configurations, along with their levels, have been summarised in the table 4. Furthermore, a sample design of diverged wall straight diffuser has also been presented in figure 14. It can be seen that the shroud wall is diverged from the diffuser inlet to one-fifth of the diffuser and is applied on the circumference of the diffuser. This is carried out to increase the radial area of the diffuser to enhance the diffuser performance. Furthermore, the diffuser outlet width has increased up to 1.4 of the diffuser inlet width. The diffuser outlet width cannot be extended more than 1.4 because of the limitation on the volute inlet section. The results obtained from the diverged wall diffuser have been compared with the straight diffuser to investigate the performance improvement within the compressor stage. Based upon the Full Factorial based DoE 24 number of numerical simulations has been required to carry out this parametric investigation. The total-to-total pressure ratio and isentropic efficiency have been recorded for each simulation. Best design model has been chosen based upon the highest localised isentropic efficiency within the compressor stage, which is the function of various geometrical and flow parameters.

Table 4. Factors and levels for full factorial design of diffuser configurations

Factors	L/L_{max}	b_2/b_1
Level 1	0.0	1.1
Level 2	0.1	1.2
Level 3	0.2	1.3
Level 4	0.3	1.4
Level 5	0.4	-
Level 6	0.5	-

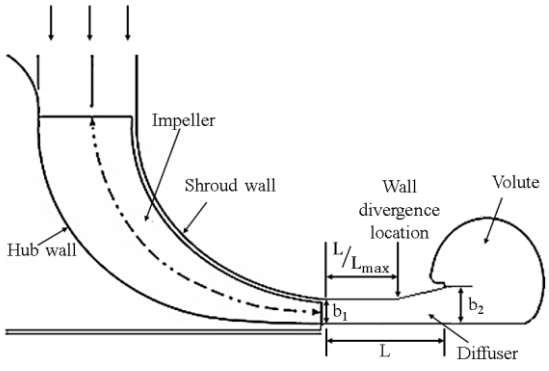

Figure 14. Sample configuration of the diverged wall vaneless diffuser

Numerical analysis has been carried out to obtain the total-to-total stage performance and flow field characteristics across various configurations of the diverged wall straight diffuser have been analysed. Table 5 shows the results obtained from numerical simulations of CFD for the global parameters of all 24 configurations. Two geometrical parameters are considered, divergence location from the inlet on the shroud wall and the diffuser outlet-to-inlet width ratio to analyse the effect on the local flow field and on the total-to-total stage performance. It can be seen from the table 2 that a small increase of outlet-to-inlet width ratio causes increase in the pressure ratio and the isentropic efficiency. However, with a further increase of outlet-to-inlet width ratio causes reduction in the stage performance. Furthermore, change in the location of wall divergence has a very small effect on the global performance parameters. However, local flow fields within the diffuser do change, which are explained in the later sections. Furthermore, it can be seen that the pressure ratio and isentropic efficiency is maximum at three diverged wall diffuser configurations; Configuration 9 (L/L_{max} = 0.2 and b_2/b_1 = 1.1), Configuration 13 (L/L_{max} = 0.3 and b_2/b_1 = 1.1) and Configuration 17 (L/L_{max} = 0.4 and b_2/b_1 = 1.1). Therefore, it can be concluded that efficiency increases with small increase of b_2/b_1 to 1.1. Increasing it more reduces the efficiency. Similarly, L/L_{max} has a significant effect from 0.2 to 0.4. The efficiency reduces as L/L_{max} is either below 0.2 or higher than 0.4. To analyse the flow behaviour across diverged wall diffuser detailed analysis is required to quantify the effect of L/L_{max} and b_2/b_1.

Table 5. CFD results of centrifugal compressor stage using different configurations of diverged wall vaneless diffuser

Parameters	Divergence location from the inlet on the shroud wall, L/L_{max}	Diffuser outlet-to-inlet width ratio, b_2/b_1	Pressure Ratio, PR_C	Isentropic efficiency, η
Configuration No.	(-)	(-)	(-)	(%)
Straight diffuser	0.0	1.0	1.527	70.9
1	0.0	1.1	1.542	72.3
2		1.2	1.536	71.6
3		1.3	1.531	71.0
4		1.4	1.522	69.9
5	0.1	1.1	1.542	72.3
6		1.2	1.536	71.6
7		1.3	1.531	71.0
8		1.4	1.521	69.9
9	0.2	1.1	1.543	72.3
10		1.2	1.536	71.6
11		1.3	1.532	71.1
12		1.4	1.522	69.9
13	0.3	1.1	1.543	72.3
14		1.2	1.537	71.7
15		1.3	1.533	71.2
16		1.4	1.523	70.1
17	0.4	1.1	1.543	72.3
18		1.2	1.537	71.6
19		1.3	1.534	71.2
20		1.4	1.525	70.2
21	0.5	1.1	1.534	71.3
22		1.2	1.537	71.6
23		1.3	1.529	70.7
24		1.4	1.522	69.8

4.4. Flow Field Analysis within Diverged Wall Straight Diffuser

Figure 15 depicts the flow streamlines radially across (a) parallel wall diffuser and diverged wall straight diffuser configurations ((b) L/L_{max} = 0.0 and b_2/b_1 = 1.1, (c) L/L_{max} = 0.1 and b_2/b_1 = 1.2, (d) L/L_{max} = 0.2 and b_2/b_1 = 1.3 and (e) L/L_{max} = 0.3 and b_2/b_1 = 1.4) at BEP at an operational speed of 58.9rpsK$^{-1/2}$. It can be seen from figure 15(a) that the flow stream within the parallel wall diffuser is uniform, with no flow reversals. Similar flow behaviour is obtained in diverged wall straight diffuser of L/L_{max} = 0.0 and b_2/b_1 = 1.1. Furthermore, it can be seen a further increase of outlet-to-inlet width ratio along with an increase in the distance between the divergence location and the diffuser inlet has caused flow reversals within the diffuser near the diffuser outlet and in the volute. Same flow behaviour has been obtained in the diverged wall diffuser configuration of L/L_{max} = 0.1 and b_2/b_1 = 1.2, L/L_{max} = 0.2 and b_2/b_1 = 1.3 and L/L_{max} = 0.3 and b_2/b_1 = 1.4. It can be seen from the figures that increase in the outlet-to-inlet width ratio has increased cross sectional area, which in-turn increases the flow reversals area. Furthermore, it can also be seen that increase in the distance between the divergence location and the diffuser inlet has shifted the flow separation point on the hub wall. It has been analysed from these flow behaviours within diverged wall diffuser configurations that increased area ratio causes increase in the adverse pressure gradient on the hub wall. The adverse pressure gradient values away from zero causes the flow separation [28]. Furthermore, the location of separation point is dependent upon the velocity gradient normal to the hub wall. When the velocity gradient is equal to zero (dw/dx = 0), it causes wall shear stress to be zero. Furthermore, the location where the velocity gradient normal to the surface is zero is known as flow separation point. This thickens the boundary layer along with flow separation region [28] and hence causes blockage, which can be captured at the flow separation point [29].

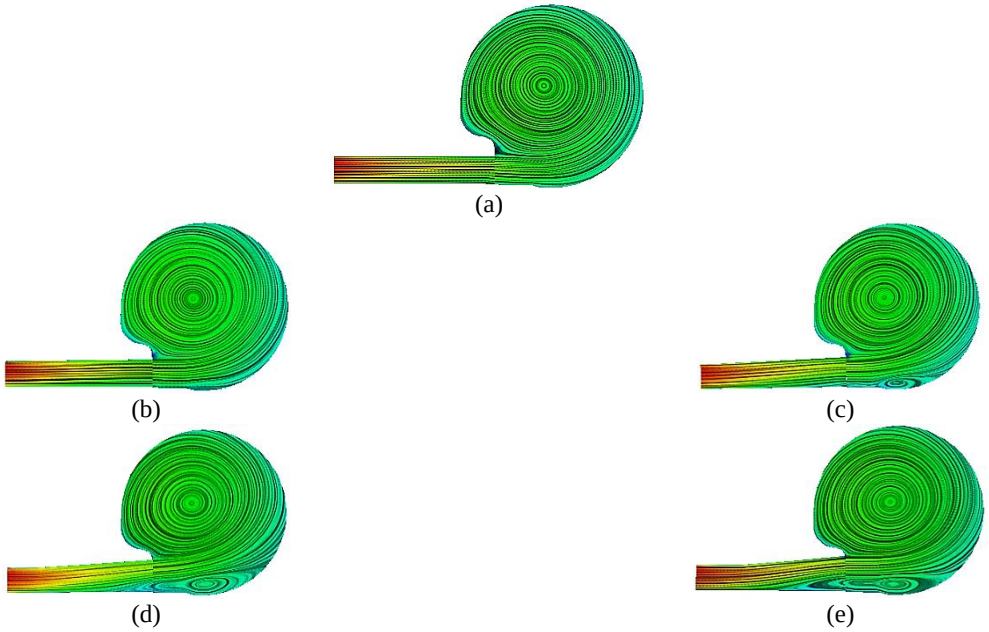

Figure 15. Flow streamlines radially across the (a) parallel wall diffuser and diverged wall straight diffuser configurations ((b) L/L_{max} = 0.0 and b_2/b_1 = 1.1 (c) L/L_{max} = 0.1 and b_2/b_1 = 1.2, (d) L/L_{max} = 0.2 and b_2/b_1 = 1.3 and (e) L/L_{max} = 0.3 and b_2/b_1 = 1.4) and volute at BEP an operational speed of 58.9rpsK$^{-1/2}$

The analysis has also been carried out in order to observe the flow characteristics circumferentially within the diverged wall straight diffuser and volute. In order to qualitatively analyse the flow characteristics many planes have been created at every 45˚ within the diffuser and volute for the design configuration of L/L_{max} = 0.3 and b_2/b_1 = 1.4. Streamlines have been shown on each plane of the diffuser and the volute (shown in figure 16). It can be seen from the figures that the size of the flow reversals and location of flow separation changes based upon the cross-sectional area of the volute. If the volute cross-sectional area is small, the size of the flow reversals is large and vice versa.

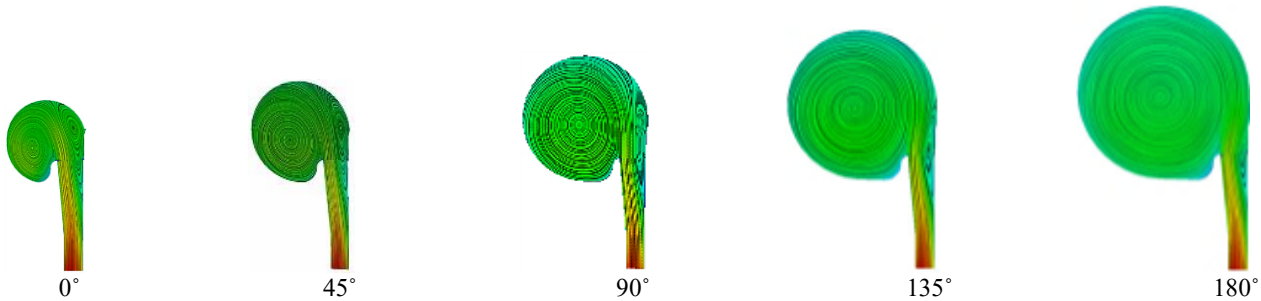

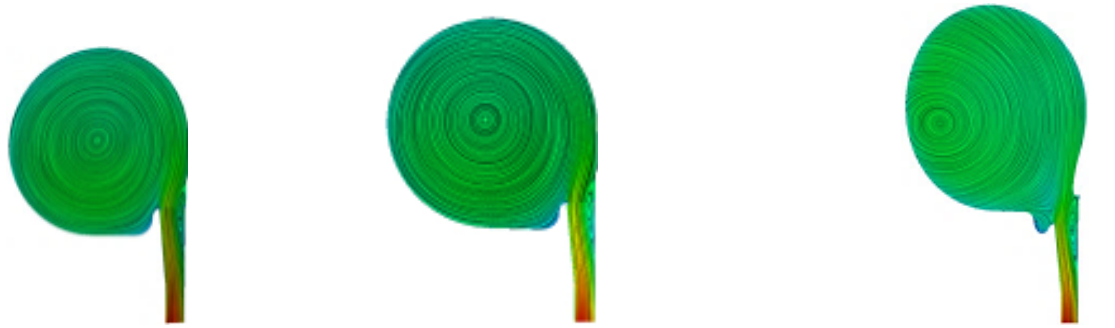

Figure 16. Flow streamlines radially across the diverged wall straight diffuser configuration of L/Lmax = 0.3 and b2/b1 = 1.4 and volute for every 45˚ at BEP at an operational speed of 58.9rpsK$^{-1/2}$

Figure 17 depicts the comparison of velocity magnitude distribution across parallel wall and diverged wall straight diffuser configurations (L/L_{max} = 0.0 and b_2/b_1 = 1.1 and L/L_{max} = 0.0 and b_2/b_1 = 1.4) from the hub wall to the shroud wall at BEP at an operational speed of 58.9rpsK$^{-1/2}$. It can be seen that the velocity magnitude is reduced radially across the diffuser. It can be seen that the velocity magnitude at L_1 (diffuser inlet) is similar at parallel and diverged wall straight diffusers, whereas the velocity magnitude is lower at L_5 (diffuser outlet) for diverged wall diffuser configurations in comparison to parallel wall diffuser. Furthermore, it has been observed that the velocity magnitude is asymmetric across the parallel and diverged wall straight diffuser. Moreover, it can be seen from the figure that the velocity magnitude becomes highly asymmetric across the diverged wall diffuser configuration of L/L_{max} = 0.0 and b_2/b_1 = 1.4. This is due to flow reversals at the outlet of diverged wall straight diffuser. However, the detailed analysis has been carried out by quantifying the asymmetric ratio for the velocity magnitude profile across the diverged wall diffusers.

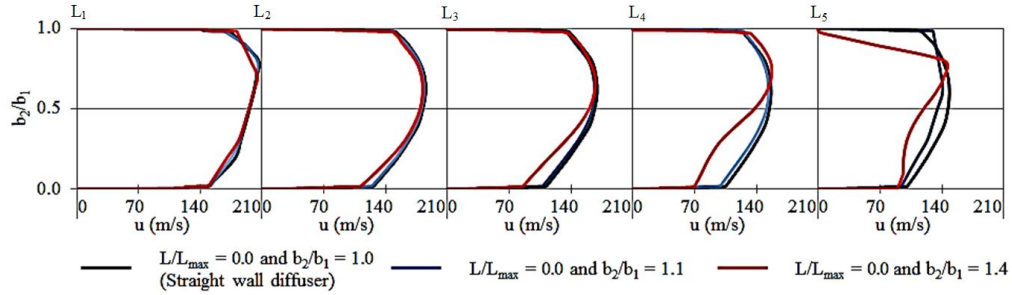

Figure 17. Comparison of velocity magnitude (m/s) distribution across parallel wall and diverged wall straight diffuser configurations from the hub wall to the shroud wall at BEP at an operational speed of 58.9rpsK$^{-1/2}$

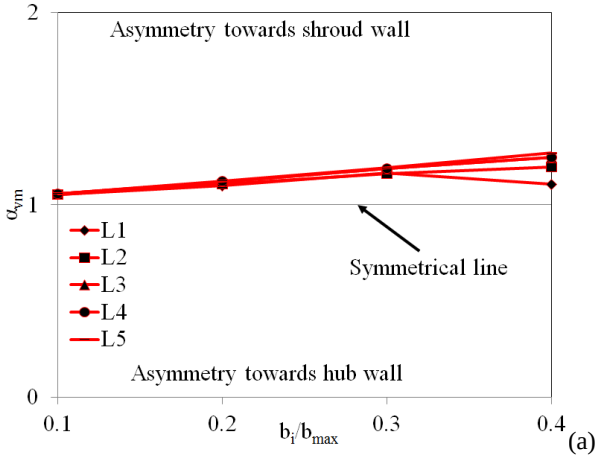

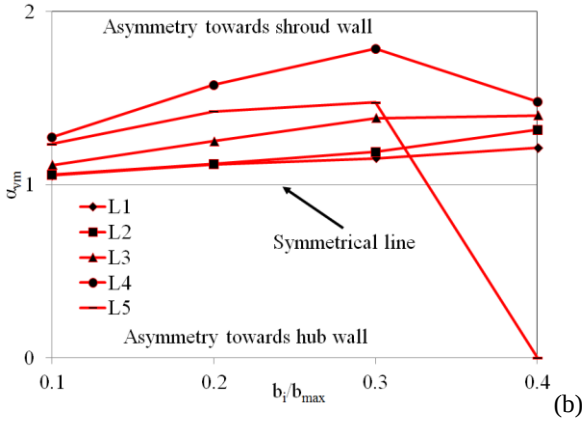

Figure 18. Local asymmetric ratio for the velocity magnitude, α_{vm} across the diverged wall diffusers ((a) L/L_{max} = 0.0 and b_2/b_1 = 1.1 and (b) L/L_{max} = 0.0 and b_2/b_1 = 1.4) at BEP at an operational speed of 58.9rpsK$^{-1/2}$

The behaviour of velocity magnitude across the diverged wall straight diffuser is explained using symmetric and asymmetric

behaviour of the velocity field profiles. Figure 18 depicts the local asymmetric ratio for the velocity magnitudes, α_{vm} across the diverged wall diffusers (L/L_{max} = 0.0 and b_2/b_1 = 1.1 and L/L_{max} = 0.0 and b_2/b_1 = 1.4) at BEP at an operational speed of 58.9rpsK$^{-1/2}$. α_{vm} values of 1.0 shows the flow is symmetric, α_{vm} values below 1.0 shows asymmetric flow towards the hub wall and α_{vm} values above 1.0 shows asymmetric flow towards the shroud wall. It can be seen that the flow is asymmetric towards the shroud wall across the diverged wall diffuser. The asymmetric ratio for the velocity magnitude increases from the centreline of the diffuser towards the wall and from the diffuser inlet to the diffuser outlet in both diverged wall diffusers. However, it has been noticed that increase of outlet-to-inlet width ratio by considering same wall diverged location from the inlet makes the flow highly asymmetrical.

Figure 19 depicts the comparison of velocity magnitude distribution across parallel wall and diverged wall straight diffuser configurations (L/L_{max} = 0.0 and b_2/b_1 = 1.4 and L/L_{max} = 0.3 and b_2/b_1 = 1.4) from the hub wall to the shroud wall at BEP at an operational speed of 58.9rpsK$^{-1/2}$. It can be seen that the velocity magnitude is reduced radially across the diffuser. It can be seen that the velocity magnitude at L_1 (diffuser inlet) is similar at parallel and diverged wall straight diffusers, whereas the velocity magnitude is lower at L_5 (diffuser outlet) for diverged wall diffuser configurations in comparison to parallel wall diffuser. Furthermore, it has been observed that the velocity magnitude is asymmetric across the parallel and diverged wall straight diffuser. Moreover, it can be seen from the figure that the velocity magnitude becomes highly asymmetric across both diverged wall diffuser configurations analysed. This is due to flow reversals at the outlet of diverged wall straight diffuser. However, the detailed analysis has been carried out by quantifying the asymmetric ratio for the velocity magnitude profile across the diverged wall diffusers.

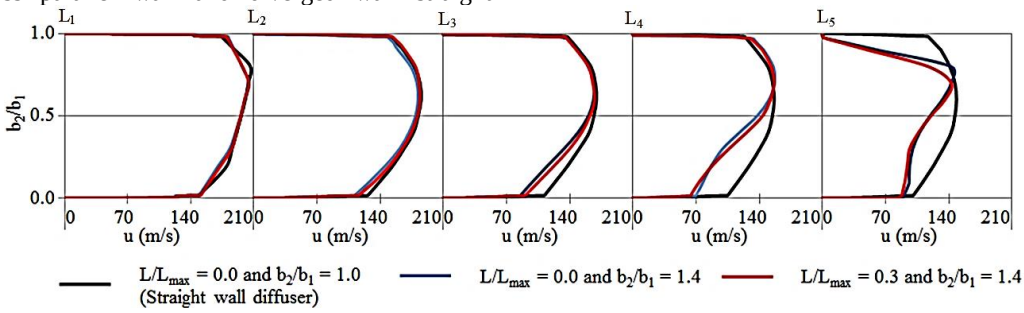

Figure 19. Comparison of velocity magnitude (m/s) distribution across parallel wall and diverged wall straight diffuser configurations from the hub wall to the shroud wall at BEP at an operational speed of 58.9rpsK$^{-1/2}$

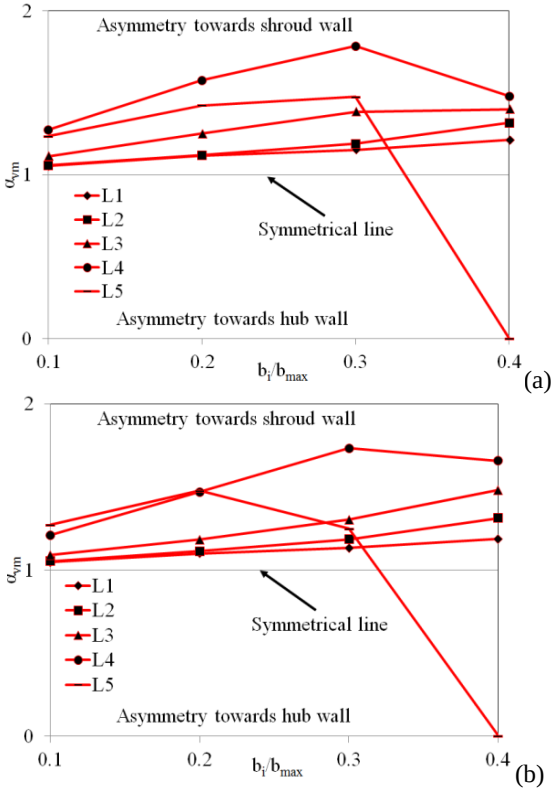

Figure 20. Local asymmetric ratio for the velocity magnitude, α_{vm} across the diverged wall diffusers ((a) L/L_{max} = 0.0 and b_2/b_1 = 1.4 and (b) L/L_{max} = 0.3 and b_2/b_1 = 1.4) at BEP at an operational speed of 58.9rpsK$^{-1/2}$

Figure 20 depicts the local asymmetric ratio for the velocity magnitudes, α_{vm} across the diverged wall diffusers (L/L_{max} = 0.0 and b_2/b_1 = 1.4 and L/L_{max} = 0.3 and b_2/b_1 = 1.4) at BEP at an operational speed of 58.9rpsK$^{-1/2}$. It can be seen that the flow is asymmetric towards the shroud wall across the diverged wall diffusers. The asymmetric ratio for the velocity magnitude remains similar from the centreline of the diffuser towards the wall and from the diffuser inlet to the diffuser outlet in both diverged wall diffusers. However, it has been noticed that by increasing wall diverged location from the inlet and considering same increase of outlet-to-inlet width ratio do not have considerable effect on the asymmetry of the flow within the diffuser.

Figure 21 depicts the comparison of velocity magnitude distribution across parallel wall and diverged wall straight diffuser configurations (L/L_{max} = 0.0 and b_2/b_1 = 1.1, L/L_{max} = 0.1 and b_2/b_1 = 1.2, L/L_{max} = 0.2 and b_2/b_1 = 1.3, L/L_{max} = 0.3 and b_2/b_1 = 1.4) from the hub wall to the shroud wall at BEP at an operational speed of 58.9rpsK$^{-1/2}$. It can be seen that the velocity magnitude is reduced radially across the diffuser. It can be seen that the velocity magnitude at L_1 (diffuser inlet) is similar at parallel and diverged wall straight diffusers, whereas the velocity magnitude is lower at L_5 (diffuser outlet) for diverged wall diffuser configurations in comparison to parallel wall diffuser. Furthermore, it has been observed that the velocity magnitude is asymmetric across the parallel and diverged wall straight diffuser. Moreover, it can be seen that the flow asymmetry for velocity magnitude is increasing with the combined increase of diffuser outlet-to inlet width ratio and wall divergence location from the inlet. However, the detailed analysis has been carried out by quantifying the asymmetric ratio for the velocity magnitude profile across the diverged wall diffusers, which has been explained in the next sections.

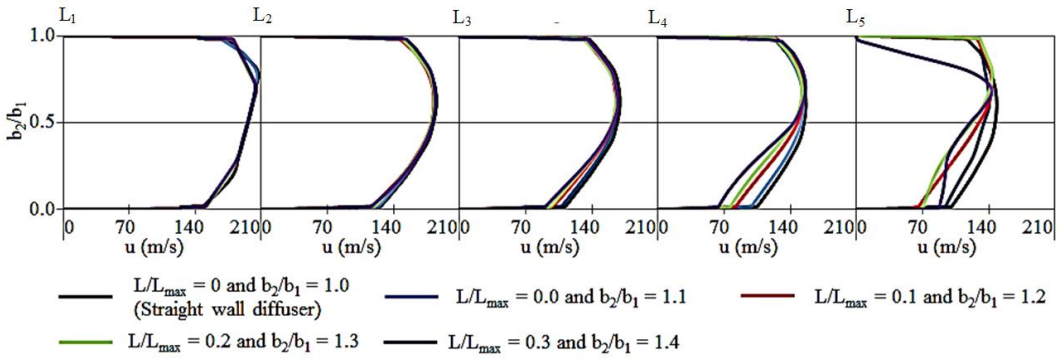

Figure 21. Comparison of velocity magnitude (m/s) distribution across parallel wall and diverged wall straight diffuser configurations from the hub wall to the shroud wall at BEP at an operational speed of 58.9rpsK$^{-1/2}$

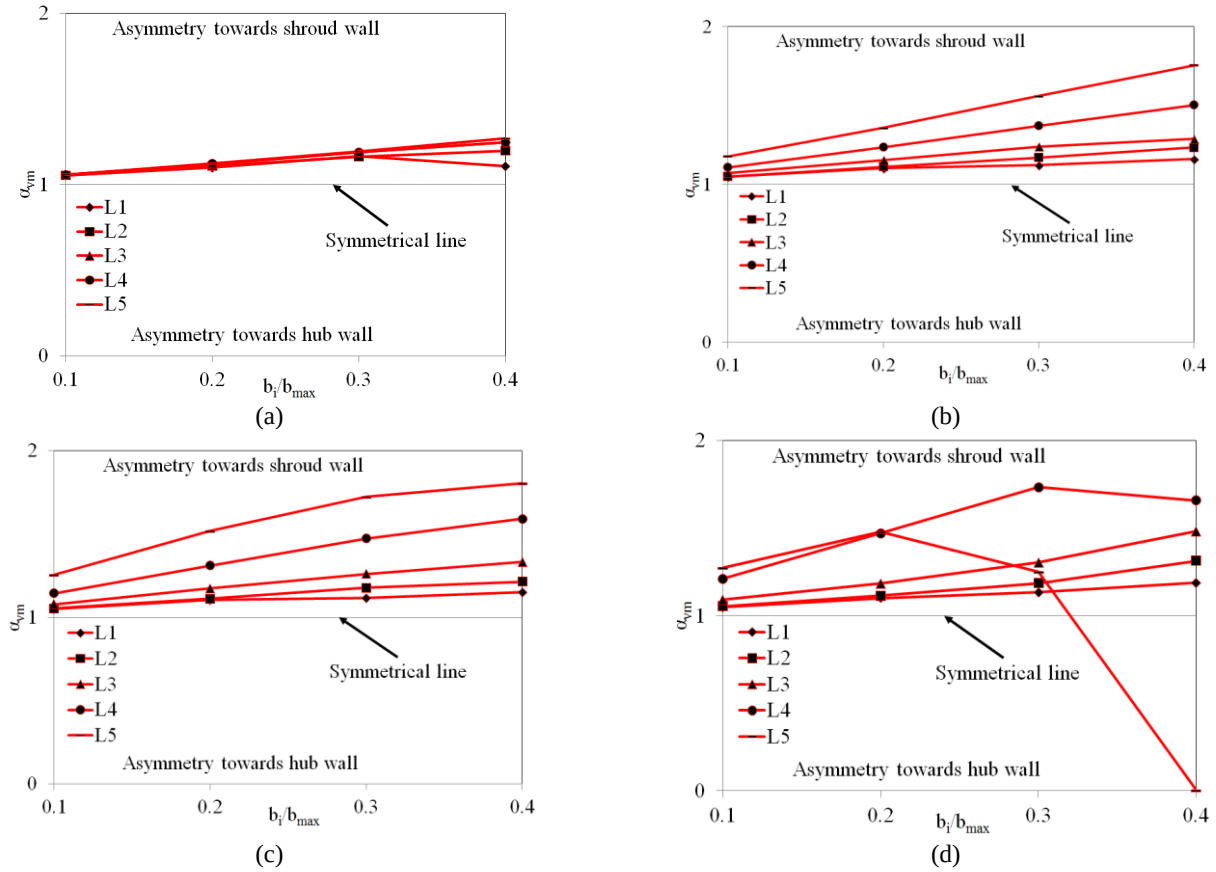

Figure 22. Local asymmetric ratio for the velocity magnitude, αvm across the diverged wall diffusers ((a) L/Lmax = 0.0 and b2/b1 = 1.1, (b) L/Lmax = 0.1 and b2/b1 = 1.2, (c) L/Lmax = 0.2 and b2/b1 = 1.3 and (d) L/Lmax = 0.3 and b2/b1 = 1.4) at BEP at an operational speed of 58.9rpsK-1/2

Figure 22 depicts the local asymmetric ratio for the velocity magnitudes, α_{vm} across the diverged wall diffusers (L/L_{max} = 0.0 and b_2/b_1 = 1.1, L/L_{max} = 0.1 and b_2/b_1 = 1.2, L/L_{max} = 0.2 and b_2/b_1 = 1.3 and L/L_{max} = 0.3 and b_2/b_1 = 1.4) at BEP at an operational speed of 58.9rpsK$^{-1/2}$. It can be seen that the flow is asymmetric towards the shroud wall across the diverged wall diffusers. The asymmetric ratio for the velocity magnitude constantly increases from the centreline of the diffuser towards the wall and from the diffuser inlet to the diffuser outlet in both diverged wall diffusers. However, it has been noticed that increasing both wall diverged location from the inlet and outlet-to-inlet width ratio increases local asymmetric ratio of the flow within the diffuser. It can also be observed that at diverged wall diffuser of L/L_{max} = 0.3 and b_2/b_1 = 1.4, the flow near the wall has asymmetry towards the hub wall.

5. Results and Discussions

5.1. Asymmetric Effect within Straight and Diverged Wall Diffuser

The behaviour of the flow within the diffuser is highly dependent upon the mass flow rate the compressor stage is working on. It has been noticed in the previous section that at near choke condition the flow is asymmetrical towards diffuser hub wall. Furthermore, the asymmetrical behaviour of the flow shifts from asymmetry towards diffuser hub wall to the diffuser shroud wall as the compressor working point changes from near choke condition to near surge condition. Therefore, a new term is introduced that shows the change in behaviour of the flow across the diffuser for different mass flow rates. The asymmetric ratio of the flow is defined as α, which is the ratio between the flow

velocity near the shroud wall and the flow velocity near the hub wall. This ratio defines the gradient of asymmetric flow behaviour across the diffuser. The average value of asymmetric ratio at one cross sectional area of the diffuser is defined as global asymmetric ratio, ξ, written as follows;

$$\xi = \frac{1}{2}\left[\frac{\alpha_1 b_1+\alpha_2 b_2+\alpha_3 b_3+\alpha_4 b_4}{b_t}\right] \quad (3)$$

where, a is the ratio of the velocity at the top and velocity at the bottom as shown in Figure 6 and b is the diffuser width. Furthermore, the subscripts 1, 2, 3 and 4 are width locations from the wall, which are explained earlier in the previous section and subscript t stands for total. The global asymmetric ratio for different velocity vectors across the diffuser are described in the following section. Furthermore, the major effects of velocity vectors on the design and off-design conditions are described in detail.

Figure 23 depicts the global asymmetric ratio for the velocity magnitude at the design and off-design conditions at an operational speed of 58.9rpsK$^{-1/2}$. It can be seen that the global asymmetric ratio for the velocity magnitudes at the design and off-design conditions is towards the shroud wall of the diffuser. The global asymmetric ratio for the velocity magnitudes is higher at L_1 (diffuser inlet) and it is decreasing towards L_5 (diffuser outlet) at BEP. Furthermore, the global asymmetric ratio for the velocity magnitudes is higher at L_1 (diffuser inlet) and it is decreasing towards L_4 at off-design conditions similar to BEP. However, asymmetric ratio increases at L_5 (diffuser outlet) at off-design conditions. The asymmetric ratio values are almost similar for BEP and near surge condition, which means flow is highly asymmetric. On the other hand, the asymmetric ratio values are lower at near choke condition, which means flow is close to symmetric.

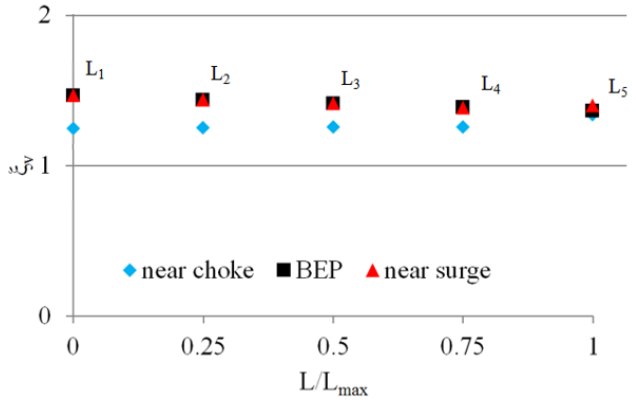

Figure 23. Global asymmetric ratio for the velocity magnitude at the design and off-design conditions at an operational speed of 58.9rpsK$^{-1/2}$

Figure 24 depicts the global asymmetric ratio for the velocity magnitude at the design and off-design conditions at an operational speed of 78.6rpsK$^{-1/2}$. It shows the same trend in comparison to that at an operational speed of 58.9rpsK$^{-1/2}$. It can be seen that the global asymmetric ratio for design and off-design conditions is towards the shroud wall of the diffuser. The global asymmetric ratio for the velocity magnitudes is higher at L_1 (diffuser inlet) and it is decreasing towards L_5 (diffuser outlet) at BEP and at near surge condition. However, the global asymmetric ratio for the velocity magnitudes is lower at L_1 (diffuser inlet) and it is increasing towards L_5 (diffuser outlet) at near choke condition. Furthermore, the asymmetric ratio values are almost similar for BEP and near surge condition, which means flow is highly asymmetric. On the other hand, the asymmetric ratio values are lower at near choke condition, which means flow is close to symmetric.

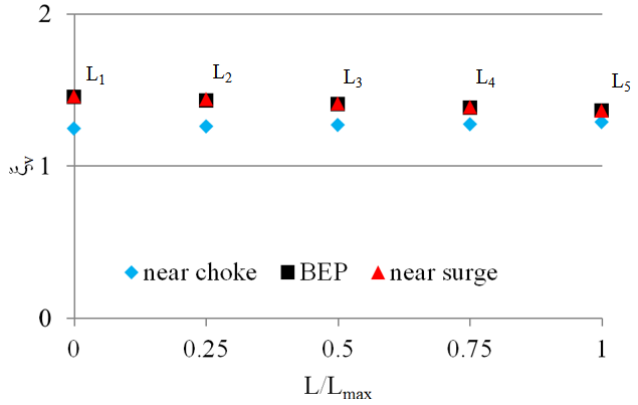

Figure 24. Global asymmetric ratio for velocity magnitude at the design and near off-design conditions at an operational speed of 78.6rpsK$^{-1/2}$

It is concluded from the above results the flow across the straight diffuser is asymmetrical at design and off-design conditions. It has been noticed that the asymmetry increases at near choke condition from the diffuser inlet to the diffuser outlet. However, the asymmetry decreases at BEP and at near surge condition from the diffuser inlet to the diffuser outlet. Furthermore, it has also been noticed that the flow tends to be more asymmetrical at the diffuser outlet at off-design conditions in comparison to BEP. This is because the diffuser has divergence on the hub wall near the outlet, which increases the area ratio of the diffuser and hence reduces the velocity. This causes the airflow to deviate towards the shroud wall of the straight diffuser. In order to understand the overall effect of the diffuser flow field on the design and off-design conditions, equation 2 has been reconsidered and manipulated to obtain the entire effect. Henceforth, a new term has been defined, which is called asymmetric effect (ζ) as follows:

$$\zeta = \frac{1}{n}\left[\frac{\xi_1 r_1+\xi_2 r_2+\xi_3 r_3+\xi_4 r_4+\xi_5 r_5}{r_t}\right] \quad (4)$$

where, n is the number of diffuser radii locations considered from the diffuser inlet and r is the diffuser radius. Furthermore, the subscripts 1, 2, 3 and 4 are radii locations from the diffuser inlet, which are 0% of distance from the diffuser inlet, 25% of distance from the diffuser inlet, 50% of distance from the diffuser inlet, 75% of distance from the diffuser inlet and 100% of distance from the diffuser inlet respectively. Moreover, subscript t stands for total. Figure 25 depicts the comparison of diffuser asymmetric effect for velocity magnitude at the design and near off-design conditions at the operational speeds of 58.9rpsK$^{-1/2}$ and 78.6rpsK$^{-1/2}$. Asymmetric effect above 1.0 shows the flow to be asymmetric towards the shroud wall within the diffuser and asymmetric effect below 1.0 shows the flow to be asymmetric towards the hub wall within the diffuser. Moreover, asymmetric effect of 1.0 shows the flow to be symmetric within the diffuser. It can be seen that the asymmetric effect is higher than 1.0 at design and near off-design conditions at the operational speeds of 58.9rpsK$^{-1/2}$ and 78.6rpsK$^{-1/2}$. Furthermore, the asymmetric effect is less at near off-design conditions in comparison to that at BEP at an operational speed of 58.9rpsK$^{-1/2}$. Moreover, the asymmetric effect is less at near choke condition in comparison to that at BEP and at near surge condition at an operational speed of 78.6rpsK$^{-1/2}$. However, it has been noticed that the velocity flow field is

highly asymmetric towards the shroud wall at BEP at the operational speeds of 58.9rpsK$^{-1/2}$ and 78.6rpsK$^{-1/2}$ in comparison to that at near off-design conditions.

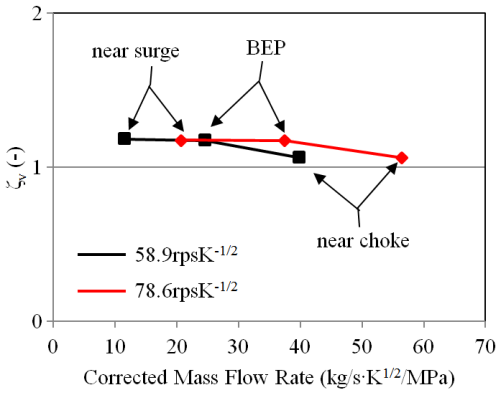

Figure 25. Comparison of diffuser asymmetric effect for velocity magnitude at the design and near off-design conditions at the operational speeds of 58.9rpsK$^{-1/2}$ and 78.6rpsK$^{-1/2}$

The behaviour of the flow within the diverged wall straight diffuser is highly dependent upon the geometrical parameter considered. It has been noticed in the previous section that increase of diffuser width ratio increases the asymmetry of the flow towards the shroud wall of the diverged wall diffuser. Furthermore, increase of divergence location on the shroud wall of the diffuser from the diffuser inlet does not affect the asymmetric behaviour of the flow. A new term is introduced that shows the change in behaviour of the flow across the diverged wall diffusers. The asymmetric ratio of the flow is defined as α, which is the ratio between the flow velocity near the shroud wall and the flow velocity near the hub wall. Equation 4.1 is used again used to obtain the global effect of diverged wall diffuser. The major effect of geometrical parameters on the asymmetric flow behaviour and stage performance is described in detail.

Figure 26 depicts the global asymmetric ratio for the velocity magnitude across the diverged wall straight diffuser at BEP at an operational speed of 58.9rpsK$^{-1/2}$. It can be seen that the global asymmetric ratio across the diverged wall diffusers is towards the shroud wall of the diffuser. The global asymmetric ratio for the velocity magnitudes is same from L_1 (diffuser inlet) to L_5 (diffuser outlet) across diverged wall diffuser of L/L_{max} = 0.0 and b_2/b_1 = 1.1 and it is decreasing from L_1 (diffuser inlet) to L_5 (diffuser outlet) across diverged wall diffuser of L/L_{max} = 0.0 and b_2/b_1 = 1.4.

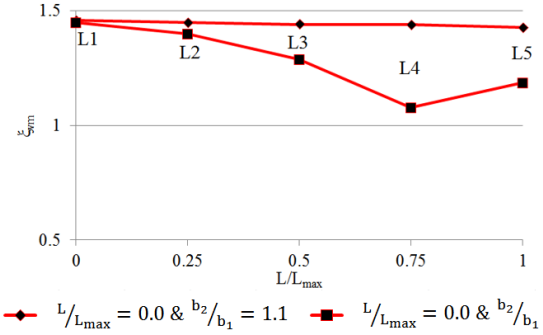

Figure 26. Global asymmetric ratio for the velocity magnitude of the diverged wall straight diffuser at BEP at an operational speed of 58.9rpsK$^{-1/2}$

Figure 27 depicts the global asymmetric ratio for the velocity magnitude across the diverged wall straight diffuser at BEP at an operational speed of 58.9rpsK$^{-1/2}$. It can be seen that the global asymmetric ratio across the diverged wall diffusers is towards the shroud wall of the diffuser. The global asymmetric ratio for the velocity magnitudes is decreasing from L_1 (diffuser inlet) to L_5 (diffuser outlet) across both diverged wall diffusers. However, it shows that diverged wall diffuser L/L_{max} = 0.3 and b_2/b_1 = 0.4 has higher global asymmetric ratio in comparison to diverged wall diffuser L/L_{max} = 0.0 and b_2/b_1 = 1.4.

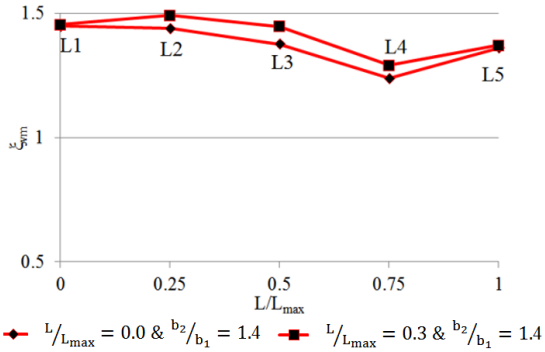

Figure 27. Global asymmetric ratio for the velocity magnitude of the diverged wall straight diffuser at BEP at an operational speed of 58.9rpsK$^{-1/2}$

Figure 28 depicts the global asymmetric ratio for the velocity magnitude across the diverged wall straight diffuser at BEP at an operational speed of 58.9rpsK$^{-1/2}$. It can be seen that the global asymmetric ratio across the diverged wall diffusers is towards the shroud wall of the diffuser. The global asymmetric ratio for the velocity magnitudes is constantly decreasing from L_1 (diffuser inlet) to L_5 (diffuser outlet) across diverged wall diffusers of L/L_{max} = 0.1 and b_2/b_1 = 1.2, L/L_{max} = 0.2 and b_2/b_1 = 1.3 and L/L_{max} = 0.3 and b_2/b_1 = 1.4. It can be analysed form this behaviour that diffusers having global asymmetric ratio decrease introduces the flow reversals within the diverged wall straight diffusers.

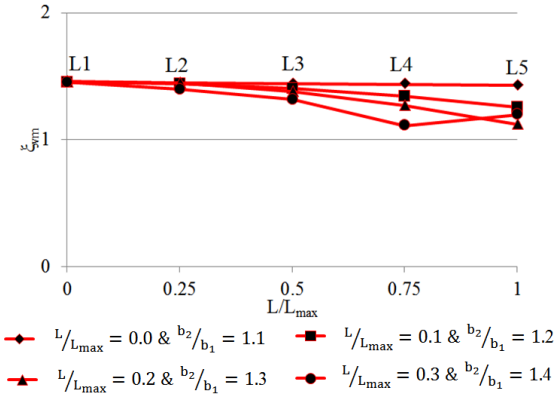

Figure 28. Global asymmetric ratio for the velocity magnitude of the diverged wall straight diffuser at BEP at an operational speed of 58.9rpsK$^{-1/2}$

Figure 29 depicts the comparison of diffuser asymmetric effect for velocity magnitude across the diverged wall straight diffusers and parallel wall diffuser at BEP at the operational speeds of 58.9rpsK$^{-1/2}$. It can be seen the diffuser asymmetric effect is reduced with the increase of outlet-to-inlet width ratio and wall divergence location form the inlet. Similar effect is obtained for the isentropic efficiency across the diverged wall diffusers. It has been concluded from the aforementioned analysis that the flow is asymmetric across the diffuser and it is increasing with the increase of outlet-to-inlet width ratio for the diverged wall straight diffusers.

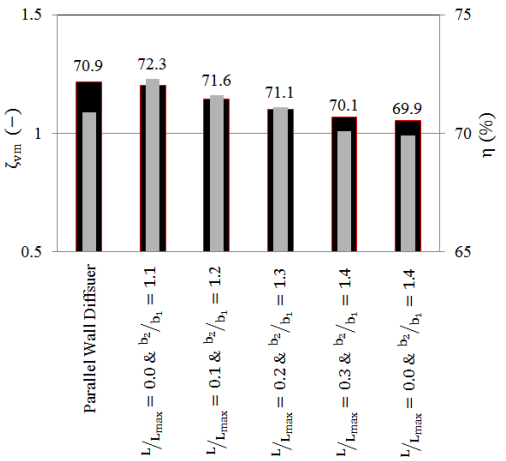

Figure 29. Comparison of diffuser asymmetric effect for velocity magnitude at the of the diverged wall straight diffusers at BEP at the operational speeds of 58.9rpsK$^{-1/2}$

5.2. Local Efficiency within Straight and Diverged Wall Diffuser

Isentropic efficiency is a non-dimensional parameter to compute the performance of the compressor stage. It is a function of the total-to-total pressure ratio and total-to-total temperature ratio of the centrifugal compressor stage, which is as follows;

$$\eta_C = \frac{T_{o,in}\times\left[PR_C^{\frac{k-1}{k}}-1\right]}{T_{o,out}-T_{o,in}} \quad (5)$$

The isentropic efficiency has been analysed locally within the diffuser at three conditions (near choke, BEP and near surge). The isentropic efficiency within the diffuser has been calculated at the locations mentioned in figure 11. Figure 30 depicts the isentropic efficiency locally within the diffuser by the method described earlier. It can be seen that 80.3% of isentropic efficiency is obtained at the diffuser inlet and it has reduced to 77.5% in the downstream of the diffuser at BEP. Furthermore, it can be seen that the trend of the isentropic efficiency is similar at near choke condition and at near surge condition. However, there are variations in the magnitude of isentropic efficiency. The isentropic efficiency values are a bit higher at the diffuser inlet at near choke condition in comparison to that at BEP and however, have same values at the diffuser outlet. This shows very less losses within the diffuser at near choke condition in comparison to that at BEP. Moreover, the isentropic efficiency values are lower across the diffuser at near surge condition in comparison to that at BEP. This shows that increased amount of losses generated while the compressor stage was working at near surge condition. These losses are due to skin friction loss, high static temperature loss and the recirculation within the diffuser.

Furthermore, a regression analysis approach is used to quantify the effects of geometrical parameters and the flow parameters on the isentropic efficiency. The flow within the diffuser is dependent on numerous factors, which could affect the isentropic efficiency locally within the diffuser of the compressor stage. The important parameters include the flow velocity components; circumferential velocity, v_θ, radial velocity, v_r and axial velocity v_a. However, axial velocity has negligible effect on the flow within the diffuser hence axial velocity component is neglected. Moreover, the diffuser is like a circular disc whereby the flow velocity is directed radially outward. Therefore, the isentropic efficiency is also the function of the geometrical parameters including inner and outer radii of the diffuser, inner and outer widths of the diffuser and azimuthal angle of the diffuser. Furthermore, the performance of the diffuser is quantified using the local isentropic efficiency considered across the diffuser. This will determine the impact of the local efficiency on the total-to-total stage efficiency. A regression analysis has been carried out to develop an equation by which isentropic efficiency can be calculated at any location within the diffuser.

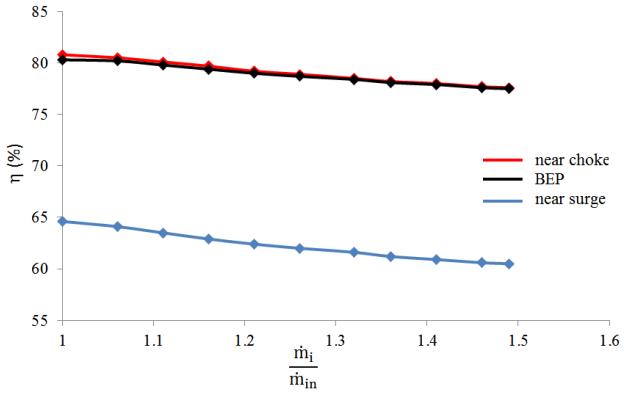

Figure 30. Isentropic efficiency locally within the diffuser at design and off-design conditions

$$\eta = f(N, \theta, r, b_2, z, \omega, T_\circ, |v|, v_\theta, v_r) \quad (6)$$

Using the regression analysis approach following equation has been developed. This expression is only valid for straight diffuser.

$$\eta = 1.82 \cdot \left(\frac{N\theta}{r}\right)^{k_1} \cdot \left(\frac{b_2 - z}{b_2}\right)^{k_2} \cdot \left(\frac{\omega r}{\sqrt{\gamma R T_\circ}}\right)^{k_3} \cdot \left(\frac{|v| - v_\theta}{|v| - v_r}\right)^{k_4} \quad (7)$$

where,

$$k_1 = 0.0023$$

$$k_2 = 0.038$$

$$k_3 = 2.26$$

$$k_4 = 0.0319$$

$N\theta/r$ and $(b_2 - z)/b_2$ are geometrical parameters considered. $N\theta/r$ helps in specifying the point across the radius of the diffuser. $(b_2 - z)/b_2$ helps to specify the location of the point across the width of the diffuser. These points are considered to obtain the efficiency at those locations. $\omega r/(\gamma RT_o)^{1/2}$ and $(|v| - v_\theta)/(|v| - v_r)$ are flow parameters considered, which have impact on the efficiency across the diffuser. $\omega r/(\gamma RT_o)^{1/2}$ is the Mach number across those points and $(|v| - v_\theta)/(|v| - v_r)$ is the ratio of circumferential velocity and radial velocity. Axial velocity does not have a significant effect on the flow, therefore has not been considered. These coefficients' values are only valid for the respective initial and boundary conditions. Furthermore, these coefficients represent the mean change in the response variable at one unit of change in the predictor variable while holding the other predictor variable in the model constant. The response variables are $N\theta/r$, $(b_2 - z)/b_2$, $\omega r/(\gamma RT_o)^{1/2}$ and $(|v| - v_\theta)/(|v| - v_r)$, whereas the predictor variable is the isentropic efficiency, η. The first term in the equation 1.82 is the y-intercept value. Furthermore, the exponent values of k_1, k_2, k_3 and k_4 are given, which shows that which term has maximum effect on the isentropic efficiency value. Henceforth, it can be seen that the maximum effect is dependent upon $\omega r/(\gamma RT_o)^{1/2}$ term. This term identifies the rotational speed of the impeller and the Mach number obtained at the impeller trailing edge tip.

The data obtained via Eq. 6 has been verified with the calculated numerical results of the isentropic efficiency, as depicted in figure 31, which has shown the maximum percentage difference of 7.01% and having R^2 value of 0.60. Based upon

this, it can be concluded that the aforementioned semi-empirical equation can predict the isentropic efficiency within the diffuser.

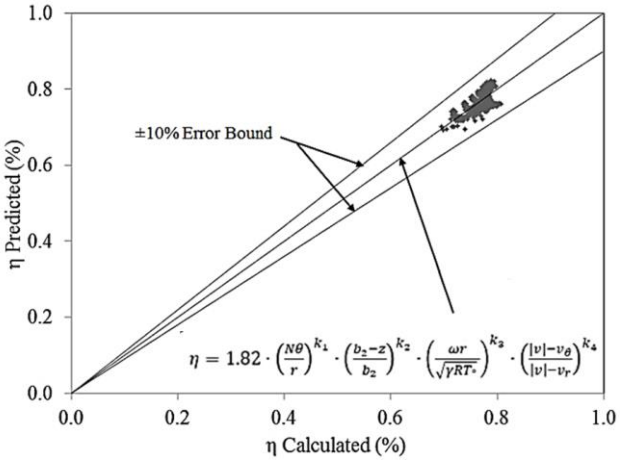

Figure 31. Comparison between numerically calculated, obtained via regression analysis, isentropic efficiency and predicted, using CFD, isentropic efficiency within the diffuser

This section comprised of the diverged wall straight diffuser performance parameters of the compressor stage. Furthermore, local isentropic efficiency is calculated within the diverged wall diffuser using regression analysis.

The analytical expression used earlier for the parallel wall diffuser has been modified by inputting one more variable of wall divergence location from the diffuser inlet with changing outlet-to-inlet width ratio. The equation is shown below. Moreover, this equation is only valid for the respective initial and boundary conditions. As the boundary conditions or initial conditions change, the coefficient values will change as well.

$$\eta = 1.82 \cdot \left(\frac{N\theta}{r}\right)^{k_1} \cdot \left(\frac{b_2-z}{b_2} \cdot \frac{N-L}{L}\right)^{k_2} \cdot \left(\frac{\omega r}{\sqrt{\gamma RT_\circ}}\right)^{k_3} \cdot \left(\frac{|v|-v_\theta}{|v|-v_r}\right)^{k_4} \quad (7)$$

where,

$$k_1 = 0.004$$

$$k_2 = 0.029$$

$$k_3 = 3.988$$

$$k_4 = 0.023$$

$((b_2 – z)/b_2 \cdot (N – L)/L)$ helps to specify the location of the point across the width of the diffuser with divergence. Furthermore, these coefficients represent the mean change in the response variable at one unit of change in the predictor variable while holding the other predictor variable in the model constant. The response variables are $N\theta/r$, $((b_2 – z)/b_2 \cdot (N – L)/L)$, $\omega r/(\gamma RT_o)^{1/2}$ and $(|v| – v_\theta)/ (|v| – v_r)$, whereas the predictor variable is efficiency, η. The first term in the equation 3.182 is known as the y-intercept value. Furthermore, $(N – L)/L$ is an additional term used in this equation. This term gives the value of one, when isentropic compression efficiency is analysed in parallel wall diffuser. Otherwise, it varies as the divergence is implemented on the shroud wall of the vaneless diffuser. Furthermore, the exponent values of k_1, k_2, k_3 and k_4 are given, which shows that which term has maximum effect on the isentropic efficiency value. Henceforth, it can be seen that the maximum effect is dependent upon $\omega r/(\gamma RT_o)^{1/2}$ term. This term identifies the rotation speed of the impeller and the Mach number obtained at the impeller trailing edge tip

The data obtained through the use of equation (7) has been verified with the CFD results as depicted in figure 32, which has shown maximum percentage difference of 44.9% and having R^2 value of 0.64. Based upon this, it can be concluded that the aforementioned semi-empirical equation can predict the isentropic efficiency within the diffuser. This high percentage difference is occurred only due to few values obtained that are far away from the actual values obtained via CFD.

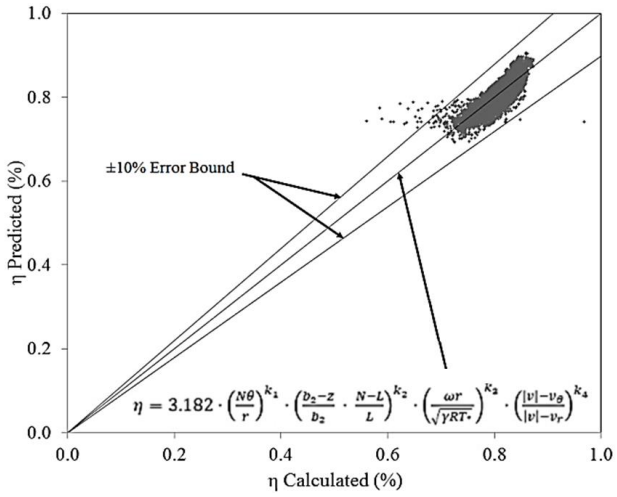

Figure 32. Comparison between numerically calculated, obtained via regression analysis, isentropic compression efficiency and predicted, using CFD, isentropic compression efficiency within the diffuser

6. Conclusions

Engine downsizing is potentially one of the most effective strategies being explored to improve fuel economy. Turbochargers are used to provide extra boost to the engine in terms of high pressure of fluid flow. A main problem of downsizing using a turbocharger is the small range of stable functioning of the turbocharger centrifugal compressor at high boost pressures. Several techniques were studied to increase the compressor operating range without sacrificing the compressor efficiency and the technique used in this study is modifying the shape of vaneless diffuser inside the compressor stage. With the advent of powerful computing machines and sophisticated software to analyse the flow fields, it has now become possible to computationally model a turbocharger compressor stage and map the flow within the centrifugal compressor stage under varying geometric and flow conditions. It has been concluded that the maximum static pressure is recovered from the straight diffuser of the compressor stage. Various results have been obtained from the analysis carried out on the straight diffuser. Static pressure fields, velocity magnitudes along with radial velocity and circumferential velocity and static temperature field results have been obtained to investigate the major effects on the flow behaviour whilst compressor is working at design and off-design conditions. It has been found that the flow within the straight diffuser is asymmetric and asymmetry is towards the shroud wall at design and off-design conditions, and at the operational speeds of $58.9 rpsK^{-1/2}$ and $78.6 rpsK^{-1/2}$. Furthermore, the local asymmetric ratio is less symmetric near the centreline of the straight diffuser and it is increasing near the wall at design and off-design conditions at the operational speeds of $58.9 rpsK^{-1/2}$ and $78.6 rpsK^{-1/2}$. Similarly, the local asymmetric ratio increases for the velocities from the diffuser inlet to the diffuser outlet at design and off-design conditions at the operational speeds of $58.9 rpsK^{-1/2}$ and $78.6 rpsK^{-1/2}$. It has also been noticed that the asymmetric effect is higher at BEP, lower at the off-design conditions at the operational speeds of $58.9 rpsK^{-1/2}$, and $78.6 rpsK^{-1/2}$. Semi-empirical equation has been developed using

regression analysis, which is used to calculate the isentropic efficiency at any point across the straight diffuser. It is found that the maximum effect is obtained on the isentropic efficiency is due to Mach number at the inlet of the diffuser.

It has been concluded from the analysis of diverged wall diffuser that the alteration of diffuser wall causes a small increase in static pressure. The local isentropic efficiency has been investigated and a semi-empirical equation has also been developed by which the isentropic efficiency can be calculated at any location within the diverged wall diffuser. Various flow phenomena have been noticed during this investigation. It has been found that increase in b_2/b_1 causes increase in the static pressure when b_2/b_1 is 1.1 and then the static pressure is reduced by increasing b_2/b_1. It is caused due to flow reversals within the diffuser. Moreover, increase in b_2/b_1 causes decrease in the static temperature, which results in increased isentropic efficiency. Increase of L/L_{max} does not have much effect on the stage performance. Diffuser asymmetric effect for the diverged wall diffusers has been investigated. It has been noticed that increase b_2/b_1 and L/L_{max} decreases the diffuser asymmetric effect. The diffuser asymmetric effect below 1.0 represents the radial flow reversals with the diverged wall diffusers. Further decrease of the diffuser asymmetric effect increases the flow reversal within the diverged wall diffusers. This causes blockage within the diverged wall diffusers. This behaviour decreases the area for the flow in the downstream direction, which increase the velocity and reduces the static pressure. An analytical expression is developed for the local isentropic efficiency within the diffuser. This expression is valid for the diverged wall diffuser. A term (N-L)/L is added that helps to calculate the isentropic efficiency based upon wall divergence location from the diffuser inlet.

References

1. Japikse, D. and Goebel, J. (1979). Turbocharger compressor performance evaluation and critical flow field measurements. SAE Transactions. 1084 – 1103.
2. Adachi, Y. Otsuki, A. Bantle, K. and Miyake, Y. (1992). Performance Improvement of a Vaneless Diffuser of Centrifugal Compressor. International Refrigeration and Air Conditioning Conference. 93 – 102.
3. Lee, Y.T. and Bein, T.W. (2002). Centrifugal compressor with vaneless diffuser. US Patent 6,382,912.
4. Turunen-Saaresti, T. Reunanen, A. and Larjola, J. (2006). Computational and experimental study of pinch on the performance of a vaneless diffuser in a centrifugal compressor. Journal of Thermal Science. Volume: 15. 306 – 313.
5. Jaatinen, A. Grönman, A. Turunen-Saaresti, T. and Röyttä, P. (2011). Effect of vaneless diffuser width on the overall performance of a centrifugal compressor. Proc. of the Institution of Mechanical Engineers, Part A: Journal of Power and Energy. Volume: 225. 665 – 673.
6. Mohtar, H. Chesse, P. and Chalet, D. (2011). Effect of a map width enhancement system on turbocharger centrifugal compressor performance and surge margin, Institution of Mechanical Engineers, Part D: Journal of Automobile Engineering. Volume: 225. 395 – 405.
7. Robinson, C., Casey, M., Hutchinson, B., and Steed, R., (2012), June. Impeller-diffuser interaction in centrifugal compressors, Proc. of ASME Turbo Expo: Turbine Technical Conference and Exposition, 767 – 777.
8. Jaatinen-Värri, A. Turunen-Saaresti, T. Röyttä, P. Grönman, A. and Backman, J. (2013). Experimental study of centrifugal compressor tip clearance and vaneless diffuser flow fields. Institution of Mechanical Engineers, Part A: Journal of Power and Energy. Volume: 227. 885 – 895.
9. Sheng, F. Chen, H. Zhu, X.C. and Du, Z.H. (2012). A three-dimensional compressible flow model for rotating waves in vaneless diffusers with unparallel walls. Institution of Mechanical Engineers, Part C: Journal of Mechanical Engineering Science. Volume: 226. 2230 – 2249.
10. Schiff, J. (2013). A preliminary design tool for radial compressors, Masters by Research thesis, Lund University, Sweden.
11. Jaatinen-Värri, A. Grönman, A. Turunen-Saaresti, T. and Backman, J. (2014). Investigation of the stage performance and flow fields in a centrifugal compressor with a vaneless diffuser. International Journal of Rotating Machinery. Volume: 2014.
12. Achilleos, P. (2014). Design optimisation of a diffuser for a turbocharger compressor stage, Masters by Research thesis, University of Huddersfield, UK.
13. Shaaban, S. (2015). Design optimization of a centrifugal compressor vaneless diffuser. International Journal of Refrigeration. Volume: 60. 142 – 154.
14. Schobeiri, M. (2005). Turbomachinery flow physics and dynamic performance. Heidelberg, Springer.
15. Cox. G.D., (2007), Recent CFD techniques applied during turbomachinery design in proc. of International Aerospace CFD Conference.
16. Cox, G., Wu, J., and Finnigan, B., (2007), January. A study on the flow around the scallops of a mixed-flow turbine and its effect on efficiency in proc. of ASME Turbo Expo 2007: Power for Land, Sea, and Air. 1017 – 1028.
17. Sbardella, L. Sayma, A.I. and Imregun, M. (2000). Semi-structured meshes for axial turbomachinery blades. International Journal for Numerical Methods in Fluids. Volume: 32. 569 – 584.
18. Sayma, A.I. Vahdati, M. Sbardella, L. and Imregun, M. (2000). Modeling of three-dimensional viscous compressible turbomachinery flows using unstructured hybrid grids. AIAA. Volume: 38. 945 – 954.
19. Asim, T. Oliveira, A. Charlton, M. and Mishra, R. (2019). Improved Design of a Multi-Stage Continuous-Resistance Trim for minimum Energy Loss in Control Valves. Energy. Volume: 174. 954 – 971.
20. Asim, T. Oliveira, A. Charlton, M. and Mishra, R. (2019). Effects of the Geometrical Features of Flow Paths on the Flow Capacity of a Control Valve Trim. Petroleum science and Engineering. Volume: 172. 124 – 138.
21. Asim, T. Algadhi, A. and Mishra, R. (2018). Effect of Capsule Shape on Hydrodynamic Characteristics and Optimal Design of Hydraulic Capsule Pipelines. Journal of Petroleum Science and Engineering. Volume: 161. 390 – 408.
22. Asim, T. Charlton, M. and Mishra, R. (2017). CFD based Investigations for the Design of Severe Service Control Valves used in Energy Systems. Energy Conversion and Management. Volume: 153. 288 – 303.
23. Asim, T. and Mishra, R. (2017). Large Eddy Simulation based Analysis of Complex Flow Structures within the Volute of a Vaneless Centrifugal Pump. Sadhana. Volume: 42. 505 – 516.
24. Asim, T. and Mishra, R. (2016). Optimal design of hydraulic capsule pipelines transporting spherical capsules. Canadian Journal of Chemical Engineering. Volume: 94. 966 – 979.
25. Asim, T. and Mishra, R. (2016). Computational Fluid Dynamics based Optimal Design of Hydraulic Capsule Pipelines Transporting Cylindrical Capsules. International Journal of Powder Technology. Volume: 295. 180 – 201.
26. Asim, T. Mishra, R. Abushaala, S. and Jain, A. (2016). Development of a Design Methodology for Hydraulic Pipelines Carrying Rectangular Capsules. International Journal of Pressure Vessels and Piping. Volume: 146. 111 – 128.
27. Jaatinen, A., (2009), Performance improvement of centrifugal compressor stage with pinched geometry or vaned diffuser, Lappeenranta University of Technology, Finland.
28. Schlichting, H. and Gersten, K. (2016). Boundary-layer theory. Springer.
29. Aungier, R.H. (2000). Centrifugal compressors: a strategy for aerodynamic design and analysis. American Society of Mechanical Engineer.